Master of Science Thesis in Electrical Engineering
Department of Electrical Engineering, Linköping University, 2023

Robust Aircraft Positioning using Signals of Opportunity with Direction of Arrival

Erik Axelsson and Sebastian Fagerstedt

LINKÖPING UNIVERSITY

Master of Science Thesis in Electrical Engineering

Robust Aircraft Positioning using Signals of Opportunity with Direction of Arrival

Erik Axelsson and Sebastian Fagerstedt

LITH-ISY-EX--23/5588--SE

Supervisor: **Robin Forsling (LiU), Niklas Weckéus (Saab)**

Examiner: **Gustaf Hendeby (LiU)**

Division of Automatic Control
Department of Electrical Engineering
Linköping University
SE-581 83 Linköping, Sweden

Abstract

This thesis considers the problem of using signals of opportunity (SOO) with known direction of arrival (DOA) for aircraft positioning. SOO is a collective name for a wide range of signals not intended for navigation but which can be intercepted by the radar warning system on an aircraft. These signals can for example aid an unassisted inertial navigation system (INS) in areas where the global navigation satellite system (GNSS) is inaccessible. Challenges arise as the signals are transmitted from non-controllable sources without any guarantee of quality and availability. Hence, it is important that any estimation method utilising SOO is robust and statistically consistent in case of time-varying signals of different quality, missed detections and unreliable signals such as outliers.

The problem is studied using SOO sources with either known or unknown locations. An extended Kalman filter (EKF) based solution is proposed for the first case which is shown to significantly improve the localisation performance compared to an unassisted INS in common scenarios. Yet, a number of factors affect this performance, including the measurement noise variance, the signal rate and the availability of known source locations. An outlier rejection mechanism is developed which is shown to increase the robustness of the suggested method. A numerical evaluation indicates that statistical consistency can be maintained in many situations even with the above-mentioned challenges.

An EKF based simultaneous localisation and mapping (SLAM) solution is proposed for the case with unknown SOO source locations. The flight trajectory and initialisation process of new SOO sources are critical in this case. A method based on nonlinear least squares is proposed for the initialisation process, where new SOO sources are only allowed to be initialised in the filter once a set of requirements are fulfilled. This method has shown to increase the robustness during initialisation, when the outlier rejection is not applicable. When combining known and unknown SOO source locations, a more stable localisation solution is obtained compared to when all locations are unknown. Applicability of the proposed solution is verified by a numerical evaluation.

The computational time increases cubically with the number of sources in the state and quadratically with the number of measurements. The time is substantially increased during landmark initialisation.

Contents

Notation

Abbreviations

Abbreviation	Meaning
AM	Artificial measurements
ANEES	Average normalized estimation error squared
ANIS	Average normalised innovation squared
CRLB	Cramér-Rao lower bound
DOA	Direction of arrival
EKF	Extended Kalman filter
FIM	Fisher information matrix
GNSS	Global navigation satellite system
IMU	Inertial measurement unit
INS	Inertial navigation system
LOS	Line of sight
NLS	Nonlinear least squares
PDF	Probability density function
RMSE	Root mean squared error
SLAM	Simultaneous localisation and mapping
SNR	Signal to noise ratio
SOO	Signals of opportunity

1 Introduction

This thesis is performed on behalf of Saab AB. The task is to investigate the usage of signals of opportunity (SOO) for aircraft positioning in environments where the global navigation satellite system (GNSS) is denied. The thesis proposes a filter based approach where the direction of arrival (DOA) for incoming signals are utilised for bearing-only localisation. The thesis considers both known and unknown signal sources, where the problem becomes a simultaneous localisation and mapping (SLAM) problem. Furthermore, the robustness of the system is analysed and measures are taken to make the state estimation more resilient against faulty measurements.

1.1 Background

The ability to navigate is fundamental to every aircraft operation. As of today, the most common aircraft localisation technique is to use GNSS in combination with an inertial navigation system (INS) to get accurate position estimates. The GNSS uses a network of orbital satellites to provide high accuracy positioning for most places on earth, with standalone errors limited to a few meters, and is by far the most common method for geopositioning. The INS on the other hand is an on-board system which measures acceleration and angular rates of a vehicle and uses the information to estimate its state. An INS/GNSS integration provide stable and smooth localisation, as the INS provides position estimates with small short time errors at a fast rate, usually at least 50 Hz, while the GNSS enables a high long term accuracy at a lower rate of 1 to 10 Hz. [1]

However, the GNSS could be inaccessible in certain environments or become subject to interference from different types of jamming devices, making localisation difficult [2]. If the GNSS signal is lost, the system relies only on the inertial mea-

surements for positioning, which have shown to be insufficient for longer flights as small errors in the inertial measurements cause the position estimate to drift over time.

SOO is a collective name for various types of signals which are not originally intended for navigation, but have shown to have potential as an alternative way of positioning. These signals can have a wide range of sources but usually originate from different kinds of radars, cellular towers or radio transmitters [3]. The SOO signals can be intercepted by the radar warning system on an aircraft and their relative DOA can be measured. Using this information, and by combining several measurements, the aircraft position relative to the signal sources could possibly be estimated through triangulation. However, challenges arise as the signals are transmitted from arbitrary, non-controllable sources, and not intended for this type of usage. Therefore, there is no guarantee for a good quality of the measurements.

1.2 Problem Statement

The problem is to investigate the possibilities of using SOO-DOA measurements as an alternative aircraft localisation method in GNSS-denied environments. The goal is to achieve a system which can improve the localisation performance compared to the unassisted INS and which is robust against measurement noise and outliers. To this end, an analysis of the performance through RMSE and statistical consistency as well as an analysis of the computational complexity is provided. The localisation problem is analysed for both known and unknown signal source locations and the results are compared against one another. The following questions will be addressed:

1. Which are the dominating factors for SOO-DOA localisation performance and robustness when SOO source locations are known?

2. Which components and processes are critical for robust SOO-DOA localisation when the SOO source locations are unknown, and how is the performance improved when some of the source locations are known?

3. How does the computational time scale in SOO-DOA with known and unknown SOO source locations, and what factors affect the computational time?

1.3 Related Work

Plenty of research has been conducted investigating different alternatives for solving the issue of navigating in GNSS-denied areas. One method for doing this is to utilize SOO in various ways for localisation. In [4], the possibilities and challenges of using SOO as an alternative in GNSS-denied areas are discussed. The

article identifies typical SOO configurations and presents three different measurement models to handle the signals, received signal strength, DOA and time difference of arrival.

Another paper on the subject is [5], where a system in proof-of-concept stage shows promising preliminary results when using SOO-DOA. The paper also discusses several requirements to achieve good positioning and proposes challenges with SOO, such as problems with phase and frequency stability since the signals are not intended for navigation. This would cause problems in time of arrival (TOA) solutions since small synchronisation mismatches could introduce large errors.

The article in [6] uses DOA with bearing only measurements to provide a review of passive tracking techniques and evaluates the performance. This article compares the standard deviation for different cases, like when the target is far away or when there are small angular changes. The papers [7] and [8] have similar approaches. In [7], the performance of different methods, such as extended Kalman filter (EKF), unscented Kalman filter and particle filter (PF), are compared against each other in a bearing-only tracking scenario. In [8], RMSE performance is evaluated based on the number of observation locations and different measurement noise.

The previously mentioned research mainly focuses on the case when the signal source locations are known. There are also several articles covering the area of GNSS-denied localisation using SOO when the signal source locations are unknown, resulting in a SLAM problem. In [9], this problem is covered on a more general level. The article gives a good overview of different SLAM methods that can be used for positioning using unknown signal source locations and discusses different types of algorithms for solving SLAM problems such as an EKF and PF.

In [3], INS is used together with SOO to reduce the effect of INS drift while GNSS is unavailable. The authors use EKF-SLAM and TOA to position an unmanned aerial vehicle (UAV) using three synchronised signal transmitters with unknown positions. In the master's thesis [10], a problem similar to what is covered in this thesis has been investigated and indicates promising performance. The thesis uses DOA from unknown radar and radio transmitters to navigate a UAV without access to GNSS and tests different set-ups with various numbers of transmitters and placements as well as different level of noise in the signals. EKF-SLAM is used to fuse INS data, which is updated at 100 Hz, with DOA measurements sampled at 10 Hz. A three dimensional model is used and in addition to azimuth angle measurements, elevation angle measurements are used to roughly estimate the distance to the landmarks. An inverse depth representation has been used to reduce the covariance of the landmark estimates before initiation. The method improves accuracy but requires a larger memory capacity as more states are introduced.

The company *BAE systems* have developed an advanced navigation system called NAVSOP that can utilise SOO such as Wi-Fi, TV, radio and mobile phone signals to provide a position with an accuracy of a few meters. The system can also learn from previously unidentified signals and GPS jammers to improve the positioning further. This shows that localisation using SOO is possible. [11].

1.4 Limitations and Delimitations

The project uses the following limitation.

- Only simulated data is used.

Furthermore, there are some delimitations which also are considered.

- A flat earth in two spatial dimensions is assumed.
- The orientation of the aircraft is assumed to be known.

These delimitations are used to limit the extent of the thesis, while the simplifications should not affect the results in a significant manner. The assumption of a flat earth is made as an aircraft already have several sensors which give information regarding the altitude. The orientation is assumed to be known as the estimated orientation of an aircraft is measured using several sensors such as a directional gyroscope and a magnetic compass and can be determined with fairly high accuracy. The slight estimation errors in the heading would likely only introduce a small offset in the positioning error. [12]

1.5 Division of Work

The work conducted during this thesis have largely been a collaboration of the two authors where both have been involved in most parts of the project. However, in order to increase efficiency, the responsibilities were divided amongst the thesis authors. Erik constructed the main implementations regarding the simulation environment. He also implemented the heatmap function and calculation of the Cramér-Rao lower bound (CRLB) and filter CRLB. Simultaneously, Sebastian first implemented the Gauss-Newton algorithm for the nonlinear least squares (NLS) and then proceeded with the filter algorithms. Thus, he constructed the main code for the EKF and EKF SLAM. Both authors also worked together with the initialisation process of the SLAM filter where several different approaches were tested. Sebastian first implemented the artificial range measurements method which was then extended with NLS by Erik.

The different aspects investigated in the simulation study were also divided where Erik mainly worked with the scenario evaluation and method of landmark initialisation, while Sebastian worked on the parameter evaluation, outlier rejection and combination of known and unknown sources. Both authors worked with the realistic scenario.

1.6 Thesis Outline

In Chapter 2, the general theory and models used for state estimation using sensor fusion are presented. Algorithms for nonlinear localisation and filtering are presented and the problem is then extended to a SLAM case. This chapter also present the metrics of evaluation which are used to evaluate the performance of the implemented method.

Chapter 3 describes the system where the theory from the previous chapter has been applied to the specific case of navigating an aircraft using SOO. A system overview shows a schematic view of the system and the specific models for INS and DOA measurements used in this thesis are described and motivated.

The simulation study presented in Chapter 4 contains a description and results of the conducted simulation experiments. In this chapter, the estimator performance, statistical consistency and computational complexity is evaluated and discussed with respect to certain aspects. This includes an analysis of the robustness of the system by testing the sensitivity to outliers and the method of initialisation. Combining known and unknown sources is also analysed using different settings. Finally, tests are also conducted to analyse the general performance for a longer test flight with a mixture of randomly distributed known and unknown signal sources, to get a more realistic evaluation of how well the method could potentially perform in a real application.

Chapter 5 contains concluding remarks of the thesis and the achieved results. It also describes the future work that is needed in order to implement the presented method in a real aircraft.

2

State Estimation

This chapter presents general theory and models used for the state estimation of an aircraft. This includes state-space models and different methods for state estimation.

2.1 Estimation Model

The state estimation is based on state-space models which aim to describe the behaviour of a real aircraft system and consists of models for the dynamics and the measurements.

2.1.1 State-Space Model

The state estimation methods used in this thesis uses a general state-space model each time sample k

$$x_{k+1} = f(x_k, u_k, w_k), \qquad \text{cov}(w_k) = Q_k, \tag{2.1a}$$
$$y_k = h(x_k) + e_k, \qquad \text{cov}(e_k) = R_k, \tag{2.1b}$$

where (2.1a) describes a dynamic model and (2.1b) a measurement model. The future state x_{k+1} is predicted using the current state x_k, given input u_k and process noise w_k and dynamic model. The measurement model relates a measurement y_k to the current state x_k. [13]

The state is defined by

$$x = \begin{bmatrix} x^1 & x^2 & v^1 & v^2 \end{bmatrix}^T, \tag{2.2}$$

where x^1, $x^2 \in \mathbb{R}^1$ denote the position and v^1, $v^2 \in \mathbb{R}^1$ the velocity in Cartesian coordinates.

2.1.2 Dead-Reckoning

Dead-reckoning is a navigation method which only utilises the dynamics of the state-space model to estimate future states. A typical dead-reckoning system is an INS, which is commonly used in various vehicles and comprises an inertial measurement unit (IMU) and a navigation processor [1]. The navigation processor uses a dynamic model as in (2.1a), which in a linear case can be defined as

$$x_{k+1} = Fx_k + G(u_k + w_k), \tag{2.3}$$

where F and G are matrices. The state x_k in the INS case consist of position, velocity, body orientation. The model input u_k consists of angular rate and acceleration and w_k is the process noise. The body orientation is an important state since it is needed to compensate for the gravity in the accelerations measurements.

The position estimate in an INS is achieved through integration of the input signals from the IMU, where noisy inputs lead to an unlimited increasing accumulation of the estimation error. This causes the state estimation to drift over time[1] and increases the estimation uncertainty for every new iteration, as illustrated in Figure 2.1.

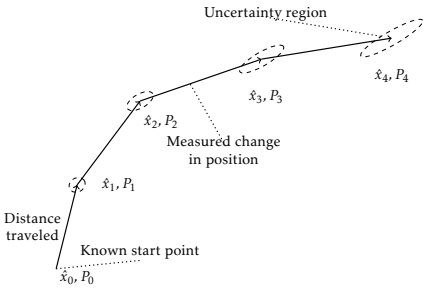

Figure 2.1: *Illustration of the increasing uncertainty of the dead-reckoning method. $\hat{x}_k$ is the estimated state, and P_k the estimated uncertainty at time k.*

2.1.3 Direction of Arrival Measurements

Direction of arrival is a method that can be used for localisation when given the angle of incoming signals. The positioning is based on lines of sight (LOS) to two

[1] The rate in which the error drifts vary, but for small systems the position error tend to be in the range of 1 to 2 nautical miles per hour. [12]

or more known signal source locations, where each LOS forms a line of possible positions and the solution is given by the intersection of the lines. The problem is illustrated in Figure 2.2.

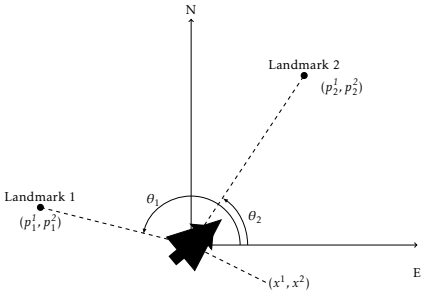

Figure 2.2: *Scematic view of the DOA measurements.*

In two dimensions, the measured angles between the receiver and a signal transmitter can be described by simple trigonometry as

$$\theta = \text{atan2}\,\frac{p^2 - x^2}{p^1 - x^1}, \tag{2.4}$$

where $p = [p^1, p^2]^T$ denotes the position of the transmitter and $x = [x^1, x^2]^T$ the position of the receiver in Cartesian coordinates. As can be seen in (2.4), the relation between the measured angle and the vehicle position is a nonlinear function, which calls for nonlinear methods to be used. Here atan2 denotes the four quadrant inverse tangent function. [1]

2.2 Nonlinear Localisation

Nonlinear least squares is a common approach for nonlinear regression. It combines observations with a model, and its estimate is defined as the solution to the optimization problem

$$\hat{x}^{NLS} = \underset{x}{\text{argmin}}\,\frac{1}{2}\sum_{k=1}^{N}\epsilon_k^2(x), \tag{2.5}$$

where k is each time-sample of N observations and the residual $\epsilon_k(x)$ is defined as

$$\epsilon_k(x) = y_k - h(x_k). \tag{2.6}$$

The derivatives of the residuals with respect to x are collected in the Jacobian $J(x)$ where

$$J(x) = \begin{bmatrix} \frac{\partial \epsilon_1}{\partial x^1} & \frac{\partial \epsilon_2}{\partial x^1} & \cdots & \frac{\partial \epsilon_N}{\partial x^1} \\ \frac{\partial \epsilon_1}{\partial x^2} & \frac{\partial \epsilon_2}{\partial x^2} & \cdots & \frac{\partial \epsilon_N}{\partial x^2} \end{bmatrix} = -\frac{\partial h^T(x)}{\partial x}. \tag{2.7}$$

To solve the optimization problem in (2.5) a numerical search method is required. One common method used for this is the Gauss-Newton algorithm, which is a local search algorithm that uses the gradient to find minima of a function. The search starts at an initial guess $\hat{x}^{(0)}$ and then iteratively takes steps with length α in the direction of the function gradient. A good initialisation is generally required, as there is a risk of the algorithm converging to local minima. The full algorithm is described in Algorithm 1. [13]

Algorithm 1 Gauss-Newton Algorithm

Require: Initial value $\hat{x}^{(0)}$, measurement function $h(x)$ and the gradient $J(x) = -\frac{\partial h^T(x)}{\partial x}$.

1: $i \leftarrow 0$
2: $\alpha^{(i)} \leftarrow 1$
3: Solve $\hat{x}^{(i+1)} = \hat{x}^{(i)} + \alpha^{(i)}(J(x)J^T(x))^{-1}J(x)(y - h(x))$
4: **if** $V(\hat{x}^{(i+1)}) > V(\hat{x}^{(i)})$ **then**
5: $\quad \alpha^{(i)} \leftarrow \alpha^{(i)}/2$
6: $\quad$ Repeat from step 3.
7: **end if**
8: **if** ($V(\hat{x}^{(i+1)}) - V(\hat{x}^{(i)}) <$ threshold, or maximum iterations reached) **then**
9: $\quad$ Terminate
10: **else**
11: $\quad i \leftarrow i + 1$
12: $\quad$ Repeat from step 2.
13: **end if**

2.3 Nonlinear Filtering

The information from the dynamic and measurement models in (2.1) can be fused together in a filter to obtain a posterior state estimate $\hat{x}_{k|k}$. The posterior distribution can be computed exactly for linear Gaussian systems by using the Kalman Filter (KF) [13]. The KF algorithm is commonly represented in a state-space form with process noise w_k and measurement noise e_k as defined in Section 2.1.1. By using the KF and measurements y_k, the best possible linear filter is obtained that minimises the covariance and results in an unbiased estimate.

2.3.1 Extended Kalman Filter

When using nonlinear models as in this thesis, the KF can be used if the nonlinear parts of the model are linearised and Gaussian noise is assumed. However, this

only approximates the optimal posterior distribution in an approach called the extended Kalman filter (EKF). The linearisation can be done based on the first order Taylor expansion around the current state estimate

$$h(x) \approx h(\hat{x}) + \frac{\partial h(\hat{x})}{\partial x}(x - \hat{x}), \tag{2.8}$$

where $\frac{\partial h(\hat{x})}{\partial x}$ is the Jacobian of $h(x)$ evaluated in $\hat{x}$.

In [13], the EKF on standard form is defined as recursive application of Algorithm 2. The algorithm divides the filter into a measurement- and time update in order to get an estimate $\hat{x}_{k|k}$ of the current state given measurements, and a prediction $\hat{x}_{k+1|k}$ of the state using a dynamic model.

Algorithm 2 EKF algorithm

Assume a dynamic model according to (2.1a), measurement model (2.1b), Jacobians $H_k = \frac{\partial h(x_k)}{\partial x_k}$ and $F_k = \frac{\partial f(x_k)}{\partial x_k}$, and additive noises w_k and e_k, the EKF is defined by the following recursion initialised with $\hat{x}_{1|0}$ and $P_{1|0}$.

1. **Measurement update**

$$S_k = H_{k|k-1} P_{k|k-1} H_{k|k-1}^T + R_k, \tag{2.9a}$$
$$K_k = P_{k|k-1} H_{k|k-1}^T S_k^{-1}, \tag{2.9b}$$
$$\epsilon_k = y_k - h(\hat{x}_{k|k-1}), \tag{2.9c}$$
$$\hat{x}_{k|k} = \hat{x}_{k|k-1} + K_k \epsilon_k, \tag{2.9d}$$
$$P_{k|k} = P_{k|k-1} - P_{k|k-1} H_{k|k-1}^T S_k^{-1} H_{k|k-1} P_{k|k-1}. \tag{2.9e}$$

2. **Time update**

$$\hat{x}_{k+1|k} = f(\hat{x}_{k|k}), \tag{2.10a}$$
$$P_{k+1|k} = F_{k|k} P_{k|k} F_{k|k}^T + Q_k. \tag{2.10b}$$

2.3.2 Simultaneous Localisation and Mapping

The idea behind simultaneous localisation and mapping (SLAM) is that, in an unknown environment and location, it is possible to build a map of the surrounding landmarks while simultaneously locating the position of a vehicle. It has been shown that there is a high degree of correlation between estimates of the location of landmarks in a map because of the common error in estimated vehicle position, and that the correlation increases with successive observations. This implies that a solution to the SLAM problem requires a joint state composed of the vehicle and landmark positions. [14]

EKF SLAM

The SLAM problem is commonly represented with a state-space model as defined in Section 2.1.1 and can be solved with an EKF, so called EKF SLAM. However, since the landmark positions need to be a part of the state, the new state becomes

$$z = \begin{bmatrix} x \\ \mathbf{m} \end{bmatrix}, \tag{2.11}$$

where x is the vehicle state, as in (2.2), and $\mathbf{m}$ are the states of the observed landmark locations in 2D Cartesian coordinates according to

$$\mathbf{m} = \begin{bmatrix} m_1 \\ m_2 \\ \vdots \end{bmatrix}, \quad m_i = \begin{bmatrix} m_i^1 \\ m_i^2 \end{bmatrix}. \tag{2.12}$$

Therefore, the measurement model in (2.1b) is updated to

$$y_k = h(x_k, \mathbf{m}_k) + e_k, \tag{2.13}$$

which gives the Jacobian

$$H_k = \begin{bmatrix} \frac{\partial h(x_k, \mathbf{m}_k)}{\partial x_k} & \frac{\partial h(x_k, \mathbf{m}_k)}{\partial \mathbf{m}_k} \end{bmatrix}. \tag{2.14}$$

The dynamic model in (2.1a) is unchanged and only updates the vehicle state x since the landmarks are stationary. The regular EKF algorithm in Algorithm 2 can then be used to recursively approximate the mean ($\mathbb{E}$) and covariance

$$\hat{z}_k = \begin{bmatrix} \hat{x}_{k|k} \\ \hat{\mathbf{m}}_k \end{bmatrix} = \mathbb{E}\begin{bmatrix} x_k \\ \mathbf{m}_k \end{bmatrix}, \quad P_{k|k} = \begin{bmatrix} P_{k|k}^{xx} & P_{k|k}^{xm} \\ P_{k|k}^{mx} & P_{k|k}^{mm} \end{bmatrix} = \mathbb{E}\left[\begin{pmatrix} x_k - \hat{x}_k \\ \mathbf{m}_k - \hat{\mathbf{m}}_k \end{pmatrix} \begin{pmatrix} x_k - \hat{x}_k \\ \mathbf{m}_k - \hat{\mathbf{m}}_k \end{pmatrix}^T \right], \tag{2.15}$$

of the joint posterior distribution and update the state when initialised with $\hat{z}_{1|0}$ and $P_{1|0}$. The aircraft and landmark states are kept separated in the time update according to

$$P_{k+1|k} = \begin{bmatrix} F_{k|k} P_{k|k}^{xx} F_{k|k}^T + Q_k & F_{k|k} P_{k|k}^{xm} \\ P_{k|k}^{mx} F_{k|k}^T & P_{k|k}^{mm} \end{bmatrix} \tag{2.16}$$

in order to obtain linear complexity in the number of landmarks, instead of cubical complexity [15]. See [13] and [15] for more details.

Landmark Association

Landmark association is the problem where measurements need to be associated with their corresponding landmark which is solved with an association algorithm. If a measurement cannot be associated with an existing landmark, a new landmark can be introduced to the map. In this thesis, the association between measurements and landmarks is assumed to be known, leading to no use of an association algorithm.

Landmark Initialisation

The SLAM algorithm usually starts with no prior knowledge of the surroundings and thus, has no initial landmarks to use for navigation. When a new landmark has been observed and shall be added to the map, the state vector is extended according to

$$z^a = \begin{bmatrix} x \\ \mathbf{m} \\ m_{new} \end{bmatrix}. \tag{2.17}$$

For scenarios where an observation gives information of all degrees of freedom of a new landmark m_{new}, it can be initialised by inverting the measurement function h in (2.13). The inverse is defined by $g(x, y)$ which is a function of the sensor position x and observations y. [16]

The covariance matrix is then updated according to

$$P^a = \begin{bmatrix} P_{xx} & P_{xm} & (G_x P_{xx})^T \\ P_{mx} & P_{mm} & (G_x P_{xm})^T \\ G_x P_{xx} & G_x P_{xm} & G_x P_{xx} G_x^T + G_y R G_y^T \end{bmatrix}, \tag{2.18}$$

where $G_x = \frac{\partial g}{\partial x}$ and $G_y = \frac{\partial g}{\partial y}$.

2.4 Estimator Evaluation Metrics

Several evaluation metrics for performance and robustness are given below. The evaluations are performed using M Monte Carlo (MC) simulations where i denotes the ith MC run.

2.4.1 Root Mean Square Error

The root mean square error (RMSE) at time k is defined as

$$RMSE_k = \sqrt{\frac{\sum_{i=1}^{M} \|x_k(i) - \hat{x}_k(i)\|^2}{M}}. \tag{2.19}$$

For an unbiased estimator, the RMSE is the square root of the variance, and thus, equal to the standard deviation of the residuals. [17]

2.4.2 Cramér-Rao Lower Bound

The Cramér-Rao Lower Bound is a theoretical value which provides a lower bound of the variance of any unbiased estimate. Though, the bound is theoretical and it may not be attainable for a finite amount of data. Furthermore, the CRLB only applies if certain regularity conditions of the likelihood function are assumed,

which are described in detail in [13].

The method utilises the Fisher information matrix (FIM) which, if measurement errors are Gaussian distributed, is defined as

$$\mathcal{I}(x) = H^T(x)R(x)^{-1}H(x), \tag{2.20}$$

where

$$H(x) = \nabla_x h(x). \tag{2.21}$$

The FIM shows that smaller measurement errors, or a larger gradient $H(x)$ yields more information from the measurement, which implies smaller estimation errors can be achieved. The CRLB states that any unbiased estimate must have a covariance matrix greater than or equal to the inverse of the FIM

$$\text{cov}(\hat{x}) \geq (\mathcal{I}(x))^{-1}. \tag{2.22}$$

This also implies a lower bound for the root mean square error of the estimate according to

$$RMSE = \sqrt{E[(x^1 - \hat{x}^1)^2 + (x^2 - \hat{x}^2)^2]} \approx \sqrt{\text{tr}(\text{cov}(\hat{x}))} \geq \sqrt{\text{tr}(\mathcal{I}^{-1}(x))}. \tag{2.23}$$

Parametric CRLB

CRLB can also be calculated for a filter approach to set a lower bound for any unbiased estimate $\hat{x}_{k|k}$. The parametric CRLB, $P_{k|k}^{CRLB}$, is a function of a specific trajectory, $x_{1:k}$, and the lower bound of the covariance can be described as

$$\text{cov}(\hat{x}_{k|k}) \geq P_{k|k}^{CRLB}(x_{1:k}). \tag{2.24}$$

The parametric CRLB is recursively calculated identically to the covariance update according to (2.9e) and (2.10b) in the Kalman filter described in Algorithm 2, but with the true state as input.

For more details regarding the CRLB, see [13].

2.4.3 Filter consistency

Filter consistency can be evaluated through analysis of the filter covariance and innovation using the average normalised error squared (ANEES) and the average normalised innovation squared (ANIS). The filter consistency is important as the filter gain is calculated using estimated error covariances and thus, is necessary for filter optimality. The ANEES is calculated for the state x with dimension n_x according to

$$\bar{\epsilon}_{x,k}^2 = \frac{1}{n_x M} \sum_{i=1}^{M} (x_{i,k} - \hat{x}_{i,k})^T P_{i,k}^{-1} (x_{i,k} - \hat{x}_{i,k}). \tag{2.25}$$

$\hat{x}_{i,k}$ is the estimate for the ground truth $x_{i,k}$ and $P_{i,k}$ is the filter covariance matrix at time k. Under the assumption that the filter is consistent, linear Gaussian and that ϵ is chi-square distributed, the test is to see whether

$$\mathbb{E}[\bar{\epsilon}_{x,k}^2] = 1 \tag{2.26}$$

can be accepted. The ANIS works in a similar manner, where the calculated innovation

$$\epsilon_k = y_k - h(x_{k|k-1}) \tag{2.27}$$

is compared to the filter estimated innovation covariance as calculated in (2.9a). The ANIS at time k is calculated according to

$$\bar{\epsilon}_{y,k}^2 = \frac{1}{n_y M} \sum_{i=1}^{M} \epsilon_{i,k}^T S_{i,k}^{-1} \epsilon_{i,k}, \tag{2.28}$$

where n_y is the dimension of the measurement vector. Again, the following should apply for a consistent filter

$$\mathbb{E}[\bar{\epsilon}_{y,k}^2] = 1, \quad \epsilon_k \sim \mathcal{N}(0, S_k), \tag{2.29}$$

where $\mathbb{E}[\epsilon_k \epsilon_I^T] = 0$ if $k \neq I$. [18]

3

Aircraft Positioning Using Signals of Opportunity

In this chapter, the theory and models presented in Chapter 2 are used for the specific case of positioning of an aircraft using SOO. This includes a description of the modelled SOO signals, signal preprocessing and system descriptions for when using known and unknown sources respectively. Furthermore, the method of initialisation used in the SLAM algorithm is described in detail.

3.1 System Overview

A schematic overview of the system can be seen in Figure 3.1. This system utilises a database of known landmarks, readings from the aircraft radar warning system and the onboard INS in an EKF filter to estimate a position that can be used in the navigation system. Since no real data is used in this thesis, the system components are represented using a simulation environment where necessary signals are created. The simulation environment is created in Matlab where arbitrary test missions can be created by entering a desired flight path and signal source locations. It produces a two dimensional flight trajectory where the position, velocity and acceleration of the aircraft is obtained at each time sample. The position and velocity provides a true state of the aircraft, while the acceleration is passed to an INS model to simulate IMU readings. Furthermore, the simulation outputs the true, global, angle between the aircraft and each of the surrounding signal sources according to (2.4), which simulates the radar readings. The simulated measurements are used as input to an EKF which fuses the INS data with radar readings, using a DOA model, to produce a state estimate that can be used for navigation. A filter using EKF SLAM is also available to handle cases when the signals source locations are not available in the database and assumed to be unknown.

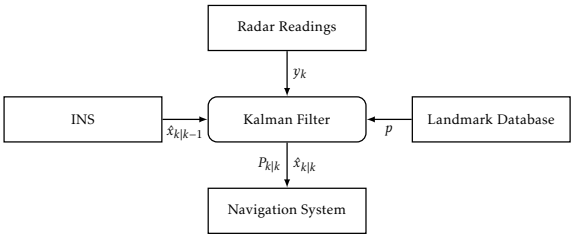

Figure 3.1: *Overview of the system.*

3.2 Signals of Opportunity

The SOO focused on in this thesis are different types of cellular towers and radars with various properties. Radars operate by rotating an antenna sending signal pulses, and the rotational speed vary for different radars. Cellular towers on the other hand, send out signals continuously in all directions. Signals from different sources can also reach different ranges, depending on the transmission power and signal frequency. In Table 3.1, a summary of the rotational speed and range of signals from different sources is presented.

Table 3.1: *Properties of some SOO. Data taken from [19], [20], [21] and [22]. These values are only used as baselines for simulations.*

	Rotational Speed [rpm]	Range [km]
4G Towers	-	1.6-19
Weather Radars	2	240
Air Surveillance Radar	12-15	75-110
Military Radar	< 480[2]	< 400[2]

Furthermore, the density of different signal sources vary. Cellular towers cover approximately 90 % of the land area in Sweden [23], while there are only 12 weather radars in total [20].

3.2.1 Signal Source Characteristics

All SOO measurements are assumed to be corrupted by independent and identically distributed noise. The maximum measurement frequency that can be used is, in the radar case, limited by the rotational speed of the sources and is calculated using

$$f_{update} = \frac{\omega}{60}, \tag{3.1}$$

[2] A rotational speed of 480 rpm and range of 400 km can not be achieved simultaneously and is only possible when focusing the radar on a smaller sector.

if the rotational speed ω is in rpm. This gives 0.033 Hz for weather radars, and a maximum of 8 Hz for the military radar. These values are used as baselines in the simulations.

The density of 4G towers is approximated by calculating the area one tower covers using

$$density \approx \frac{1}{\pi r^2}, \tag{3.2}$$

where r is the range. Here, it is assumed that 4G covers all land, and that the coverage areas do not coincide with each other. For a range of 16 kilometres, this gives a source density of $1.2 \cdot 10^{-3}$, while the density of weather radars is approximately $2.5 \cdot 10^{-5} \frac{sources}{km^2}$ in the nordics [24]. These values are used as baselines in simulations.

3.2.2 Signal Preprocessing and Outlier Rejection

The incoming signals are assumed to be pre-processed so that they can be associated with their corresponding source and the signals only contain information about the DOA. However, risk of interference and mixing of the measurements signals can occur if multiple measurements have a similar direction of arrival in real scenarios. Therefore signals are rejected according to

$$|y_{k,i} - y_{k,j}| < 3\sigma_e \tag{3.3}$$

where $i \in \{1, ..., N-1\}$, $j \in \{i+1, ..., N\}$ and N is the number of measured signals. σ_e is the standard deviation of the measurement noise for the sensor. This means that every signal $y_{k,i}$ is compared to every signal in $y_{k,j}$ individually and if the inequality in (3.3) is fulfilled, both signals are rejected.

Estimation errors can have a bigger impact when the aircraft is close to a signal source, as there is a risk of estimating a source position on the wrong side of the aircraft path. If this happens, the expected measurements become largely different from the actual angle measurements, which could corrupt the position estimate of the aircraft. The problem can occur when using known sources, but the risk is higher when unknown sources are used, as there are uncertainties both in the aircraft position and the estimated landmark positions. To reduce the risk of this happening, signals are rejected if

$$\sqrt{(\hat{x}^1 - \hat{m}_i^1)^2 + (\hat{x}^2 - \hat{m}_i^2)^2} < d_{min}, \tag{3.4}$$

is fulfilled, where d_{min} is the minimum accepted distance between the estimated aircraft and source position, $\hat{x}$ and $\hat{m}$, respectively. The minimum distance is a tuning variable, but the value 1 km has been used in this thesis.

To reduce the effect of the DOA measurement error, an outlier rejection method is implemented in the filters. The outlier rejection used is based on the normalised innovation for signal source i

$$\bar{\epsilon}_{k,i} = \frac{\epsilon_{k,i}}{\sqrt{S_{k,i}}} \sim \mathcal{N}(0,1), \tag{3.5}$$

where

$$\epsilon_{k,i} = y_{k,i} - h(x_{k|k-1}), \tag{3.6}$$
$$S_{k,i} = H_{k,i} P_{k|k-1} H_{k,i}^T + R_{k,i}, \tag{3.7}$$

is the innovation and its covariance, which is Gaussian distributed if a linear Gaussian model is used and all measurements are assumed to be inliers. This can be used since Gaussian state covariance and Gaussian measurement noise is assumed in the filter approaches. Using this, the outlier rejection is performed measurement by measurement where a measurement is considered to be an outlier if

$$\bar{\epsilon}_{k,i}^2 > \gamma, \tag{3.8}$$

is fulfilled, where γ is a threshold. The normalised innovation squared is chi-squared distributed with one degree of freedom $\chi^2(1)$, since [13]

$$\bar{\epsilon}_{k,i} \sim \mathcal{N}(0,1) \implies \bar{\epsilon}_{k,i}^2 \sim \chi^2(1). \tag{3.9}$$

The threshold γ is chosen as the $\chi^2(1)$ value corresponding to the significance level α. $p_O = 1 - \alpha$ is the probability that a measurement is correctly classified as an inlier.

3.3 INS Model

The INS model uses a constant velocity model [13], where the velocity is assumed to be constant over the sample time T. The dynamic model in (2.3) is used with F and G given by

$$F = \begin{bmatrix} 1 & 0 & T & 0 \\ 0 & 1 & 0 & T \\ 0 & 0 & 1 & 0 \\ 0 & 0 & 0 & 1 \end{bmatrix}, \quad G = \begin{bmatrix} \frac{T^2}{2} & 0 \\ 0 & \frac{T^2}{2} \\ T & 0 \\ 0 & T \end{bmatrix}. \tag{3.10}$$

In this simplified model, the input u_k only consist of acceleration measurements and the state x_k consist of position and velocity since by assumption the orientation is known. The input is defined as

$$u_k = \begin{bmatrix} a_k^1 \\ a_k^2 \end{bmatrix}, \tag{3.11}$$

where a_k^1 and a_k^2 are the true acceleration in the global x- and y-direction. The process noise w_k is assumed to be Gaussian distributed according to

$$w_k \sim \mathcal{N}(0, Q_k),$$

and consist of both noise in the acceleration measurements and model error

$$w_k = w_{k,a} + w_{k,m}. \tag{3.12}$$

Since the acceleration measurements are artificial, $w_{k,a}$ is known and modelled according to

$$w_{k,a} \sim \mathcal{N}(0, Q_{k,a}),$$

where $Q_{k,a}$ is tuned so that the INS error drift with approximately 1 nautical mile per hour. In the simulations the INS error drift mainly depend on the sampling rate and the speed of the aircraft which are constant and set to 5 Hz and 250 m/s respectively, for all simulations. This resulted in a constant $Q_{k,a} = 0.023^2 \cdot I_{2\times 2}$, which is used in all simulations.

The other part of the process noise $w_{k,m}$ is unknown and have to be accounted for in order to achieve a good estimation of the growing uncertainty

$$P_{k+1|k} = F P_{k|k} F^T + Q_k, \tag{3.13}$$

for the dead-reckoning process. In order to do this, Q_k is tuned so that the calculated ANEES according to (2.25) becomes close to 1 for 1000 Monte Carlo simulations for each scenario that is tested.

3.4 Aircraft Positioning with Known Source Locations

In Figure 3.2 a flow chart is provided that illustrates the algorithm developed for aircraft positioning using SOO-DOA with known source locations. The figure shows that a time update is done with the INS model and IMU measurements and when DOA measurement are available, they are preprocessed and used together with the measurement model to make a measurement update to achieve a position estimate that can be used in a navigation system.

In this case, the measurement model in (2.1b) is used. Since DOA measurements from SOO signals are used, the measurement function $h(x_k)$ is given by calculating (2.4) for all observed sources at time k. This gives

$$h(x_k, \mathrm{S}) = \begin{bmatrix} \operatorname{atan2} \frac{p_{s_1}^2 - x_k^2}{p_{s_1}^1 - x_k^1} \\ \vdots \\ \operatorname{atan2} \frac{p_{s_N}^2 - x_k^2}{p_{s_N}^1 - x_k^1} \end{bmatrix}, \tag{3.14}$$

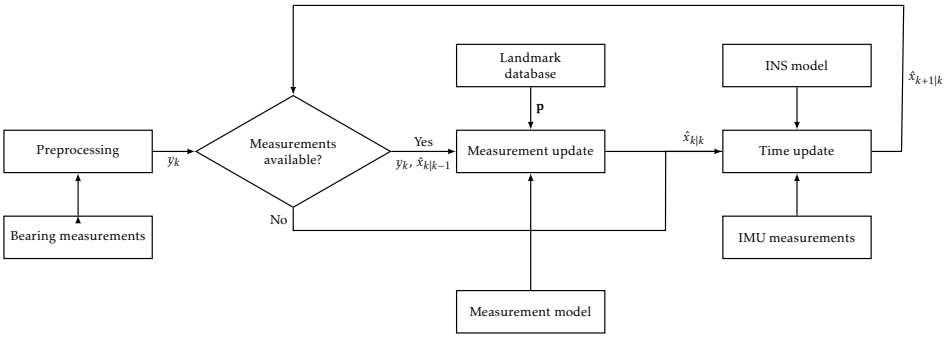

Figure 3.2: *Flow chart of the processes that occur when positioning is done with known source locations.*

and $e_k \sim \mathcal{N}(0, R_{S,k})$, where the size of $R_{S,k}$ depend on the number of observed sources. The observed sources are defined by a set $\mathrm{S} = \{s_1,...,s_N\}$ with N incoming signals at time k. S is used since all previously observed sources, further on referred as global sources, might not be observed in every sample. Thereby p_{s_n} denotes the position of a signal source with global index s_n, which is the global index of the nth observed source at time k. This is illustrated in Figure 3.3, where there are six global sources but only two observed at time k leading to $N = 2$.

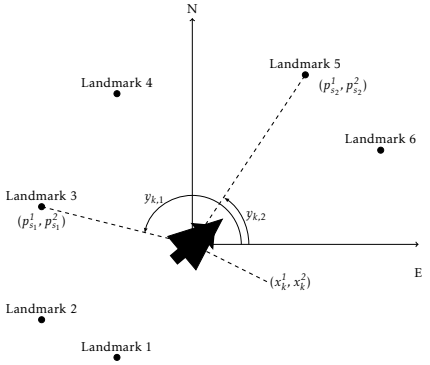

Figure 3.3: *Illustration of DOA measurements when only two out of six sources are observed. Here $s_1 = 3$ and $s_2 = 5$.*

The measurement model in (3.14) is then combined with the INS model in Section 3.3 and is used in an EKF which is implemented according to Algorithm 2. The EKF thus uses DOA measurements from sources with a known location to make a measurement update of the current state and uses acceleration measure-

ments to make a prediction of the state at the next sample. In this thesis, R_k is set to the true covariance of the measurements, while Q_k is a tuning variable which is manually set for each individual scenario as explained in Section 3.3.

The Jacobian used in Algorithm 2 becomes

$$H = \begin{bmatrix} H_1^{x^1} & H_1^{x^2} \\ \vdots & \vdots \\ H_N^{x^1} & H_N^{x^2} \end{bmatrix}, \tag{3.15}$$

$$H_n^{x^1} = \frac{\partial h_n}{\partial x^1} = \frac{p_{s_n}^2 - x^2}{(p_{s_n}^1 - x^1)^2 + (p_{s_n}^2 - x^2)^2}, \tag{3.16a}$$

$$H_n^{x^2} = \frac{\partial h_n}{\partial x^2} = \frac{x^1 - p_{s_n}^1}{(p_{s_n}^1 - x^1)^2 + (p_{s_n}^2 - x^2)^2}. \tag{3.16b}$$

3.5 Aircraft Positioning with Unknown Source Locations

When the signal source locations are unknown, an EKF SLAM approach is used instead. This method is implemented using Algorithm 2 but with the extensions described in Section 2.3.2. This requires a slightly different measurement model as well as an initialisation model in order to add new observed landmarks to the state.

In Figure 3.4, a flow chart illustrating the processes that occur when positioning is done with unknown source locations is presented. In contrast to the case with known source locations, new sources first have to go trough an initialisation process which is described more in Section 3.5.2.

3.5.1 Measurement Model

Since the sources are a part of the state, the measurement model depends on the state and the set S with N observed sources that have been initialised. This means that the measurement function in (3.14) is updated to

$$h(x_k, \mathbf{m}, \mathrm{S}) = \begin{bmatrix} \operatorname{atan2} \frac{m_{s_1}^2 - x_k^2}{m_{s_1}^1 - x_k^1} \\ \vdots \\ \operatorname{atan2} \frac{m_{s_N}^2 - x_k^2}{m_{s_N}^1 - x_k^1} \end{bmatrix}, \tag{3.17}$$

where m_{s_n} is the unknown location of the source s_n and $\mathbf{m}(\mathrm{S}) = [m_{s1}, ..., m_{s_N}]$. As opposed to from when only known sources are used, the estimated source locations are also stored in the the vector $\mathbf{m} = [m_1, ..., m_{N_{tot}}]^T$. Where N_{tot} is the total

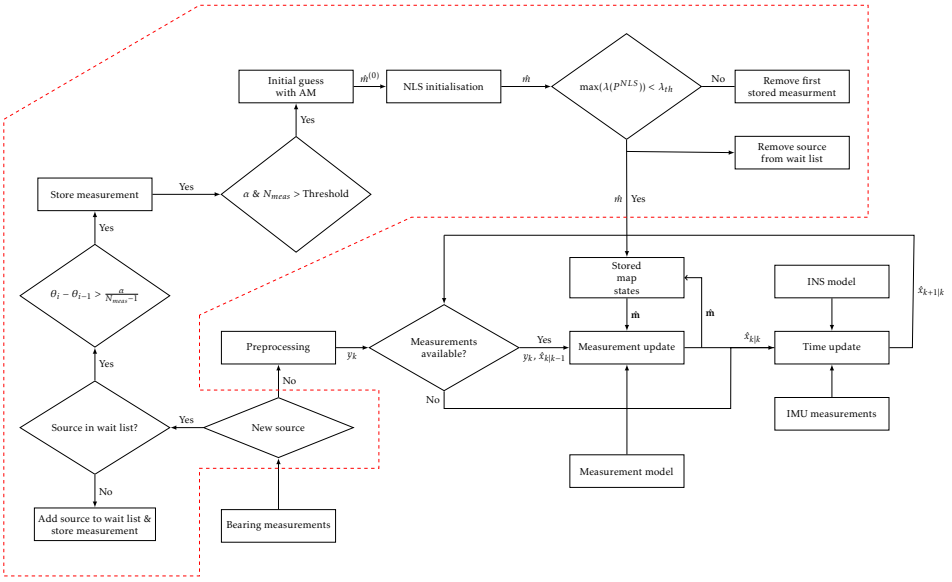

Figure 3.4: *Flow chart of the processes that occur when positioning is done with unknown source locations. The area surrounded by the red line represents the initialisation process.*

number of sources stored in the map.

The Jacobian of the measurement function with respect to x is

$$H^x = \begin{bmatrix} H_1^{x^1} & H_1^{x^2} \\ \vdots & \vdots \\ H_N^{x^1} & H_N^{x^2} \end{bmatrix}, \tag{3.18}$$

where

$$H_n^{x^1} = \frac{\partial h_n}{\partial x^1} = \frac{m_{s_n}^2 - x^2}{(m_{s_n}^1 - x^1)^2 + (m_{s_n}^2 - x^2)^2}, \tag{3.19a}$$

$$H_n^{x^2} = \frac{\partial h_n}{\partial x^2} = \frac{x^1 - m_{s_n}^1}{(m_{s_n}^1 - x^1)^2 + (m_{s_n}^2 - x^2)^2}, \tag{3.19b}$$

and since the sources now are a part of the state, the measurement model has to be derived with respect to m_{s_n} as well. This gives the Jacobian

$$H^m = \begin{bmatrix} H_1^m \\ \vdots \\ H_N^m \end{bmatrix}, \tag{3.20}$$

where

$$H_n^m = \begin{bmatrix} 0 & \dots & 0 & H_n^{m^1} & H_n^{m^2} & 0 & \dots & 0 \end{bmatrix}, \tag{3.21a}$$

$$H_n^{m^1} = \frac{\partial h_n}{\partial m_{s_n}^1} = -H_n^{x^1}, \quad H_n^{m^2} = \frac{\partial h_n}{\partial m_{s_n}^2} = -H_n^{x^2}, \tag{3.21b}$$

and s_n is the global index of the nth source as illustrated in Figure 3.3.

3.5.2 Landmark Initialisation

New landmarks are initialised into the SLAM filter as described in Section 2.3.2, where the inverse of the measurement model is used to estimate the position of a landmark. The initialisation process is divided into two parts where an artificial range measurement is used to produce an initial guess of the landmark state, which is then improved using NLS from several measurements. The methods are described in detail below.

Initialisation using Range-Bearing Measurements

For a scenario where both range and bearing are measured, making $y_k = [r_k, \theta_k]^T$, the measurement model is invertible and where the inverse $g(x_k, y_k)$, as mentioned in Section 2.3.2, is defined by

$$g(x_k, y_k) = \begin{bmatrix} x_k^1 \\ x_k^2 \end{bmatrix} + r_k \begin{bmatrix} \cos(\theta_k) \\ \sin(\theta_k) \end{bmatrix}, \tag{3.22}$$

where x_k^1, x_k^2 represent the aircraft position and r_k and θ_k are the measured range and bearing from the aircraft to the landmark at time k.
The Jacobians used in (2.18) then becomes

$$G_x = \begin{bmatrix} 1 & 0 & 0 & 0 \\ 0 & 1 & 0 & 0 \end{bmatrix}, \quad G_y = \begin{bmatrix} \cos(\theta) & -r\sin(\theta) \\ \sin(\theta) & r\cos(\theta) \end{bmatrix}. \tag{3.23}$$

The covariance R is defined as

$$R = \begin{bmatrix} R_r & 0 \\ 0 & R_\theta \end{bmatrix}, \tag{3.24}$$

where R_r is the variance of the range and R_θ is the variance of the DOA observations.

Artificial Range Measurements

However, as only information about the DOA in azimuth is provided by the SOO observations, a delayed initialisation method is used to first estimate the range using multiple observations. The estimated range can be seen as an artificial measurement of r_k and be used in (3.22) to estimate the state of the landmark. The range estimation is illustrated in Figure 3.5 and the method is described in this section.

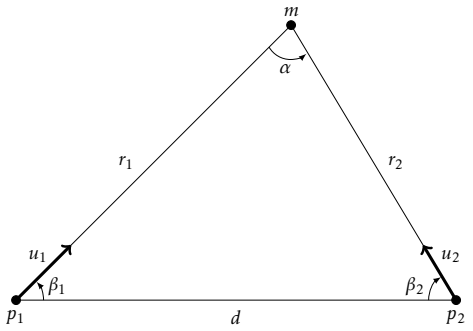

Figure 3.5: *Illustration of how the angles and vectors used to calculated the parallax α.*

In the figure, each observation point is defined as

$$p_i = \begin{bmatrix} x_i^1 \\ x_i^2 \\ \theta_i \end{bmatrix}. \tag{3.25}$$

The vectors u_1 and u_2 are unit vectors pointing in the direction of the measurement according to

$$u_i = \begin{bmatrix} \cos(\theta_i) \\ \sin(\theta_i) \end{bmatrix}. \tag{3.26}$$

Two vectors between the two observation points can also be defined as

$$d_1 = \begin{bmatrix} x_2^1 - x_1^1 \\ x_2^2 - x_1^2 \end{bmatrix}, \tag{3.27}$$

and the opposite vector $d_2 = -d_1$. The angles in the triangle is then calculated using the cross product of the vectors as

$$\beta_1 = \arcsin \frac{|d_1 \times u_1|}{\|d_1\|}, \quad \beta_2 = \arcsin \frac{|d_2 \times u_2|}{\|d_2\|}. \tag{3.28}$$

Using this information, the range r_1 is calculated as

$$r_1 = \frac{d\sin(\beta_2)}{\sin(\alpha)}, \quad r_2 = \frac{d\sin(\beta_1)}{\sin(\alpha)}. \tag{3.29}$$

The location of the landmark is calculated using (3.22) from one of the observation points. In this thesis, the range estimate from the last measurement will be used, thus $r_k = r_2$. The variance of this range measurement is estimated as [25]

$$R_{r_2} = \frac{r_2^2\cos^2(\alpha)R_\theta + r_1^2 R_\theta}{\sin^2(\alpha)}, \tag{3.30}$$

and $R_r = R_{r_2}$ is then used in (3.24). To achieve a good landmark estimate $\hat{m}$, the range is only estimated when the parallax angle α between two observations at the points p_1 and p_2 in Figure 3.5 is larger than a specified threshold value α_{th}.

NLS for Improved Initialisation

A drawback of this type of landmark initialisation is that the accuracy of the initialised landmark position becomes highly dependent on the two measurements used in the triangulation process. Thus, if one, or both, of the measurements turns out to be an outlier, the estimated landmark position risks being far off the true position, with a too optimistically estimated covariance. As a measure to reduce the risk of this happening and to increase the robustness of the system, additional measurements are stored and combined by using nonlinear least squares, as described in Section 2.2, in the initialisation. The data is stored by stacking observation points as described in (3.25) according to

$$N_{meas} = \begin{bmatrix} p_1 & p_2 & \dots & p_n \end{bmatrix}. \tag{3.31}$$

To avoid storing too many data points, only a fix number of measurements that are evenly distributed over the parallax threshold are selected. An observation point is thus only stored if

$$\theta_i - \theta_{i-1} > \frac{\alpha}{N_{meas} - 1}, \tag{3.32}$$

is fulfilled. The Gauss-Newton algorithm, as described in Algorithm 1, is then used to find the optimal landmark position given N_{meas} stored observations. The algorithm is used with an initial guess of $\hat{m}^{(0)}$ taken from (3.22) in the method described above, with p_1 and p_N as inputs.

The illustration in Figure 3.6 describes how the initial guess $\hat{m}^{(0)}$ have been corrupted by an outlier in the first measurement. When the Gauss-Newton algorithm is applied, the estimate moves in the direction of the gradient in order to minimize the cost function

$$V^{NLS}(m) = \frac{1}{2}\sum_{k=1}^{n}(y_k - h_k(x, m))^2. \tag{3.33}$$

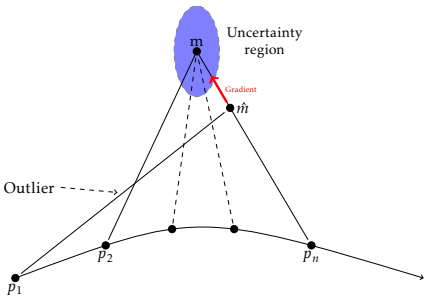

Figure 3.6: *Illustration of initialisation using NLS for several measurements. Here, a measurement outlier have corrupted the initial guess $\hat{m}$, causing a large offset. However, the weighted average of the stored measurements in the NLS creates a gradient and the Gauss-Newton algorithm pushes the estimate toward a local minima.*

By doing this, the landmark estimate becomes a weighted average of all the measurements and is thus not as sensitive to one measurement being an outlier. The estimated covariance for the NLS method can be calculated as

$$P^{NLS} = (H^T R_\theta^{-1} H)^{-1} \tag{3.34}$$

where the Jacobian H is calculated using (3.21b). This covariance is then compared to a threshold according to

$$\max(\lambda(P^{NLS})) < \lambda_{th}, \tag{3.35}$$

which is yet another measure to govern the robustness of the navigation method. The threshold stops the initialisation process if the estimated landmark covariance is too high, which could be caused by too noisy measurements or a too large distance to the source. Exceeding the threshold λ_{th} could also be a sign that bad measurements have been used in the initial guess $\hat{m}^{(0)}$, as the Gauss-Newton algorithm requires a fairly good initial guess in order to operate as intended. Therefore, the first observation, p_1 in N_{meas} is removed and the initialisation process needs to wait for a new observation before it can try again. In this thesis, $\lambda_{th} = 1 \cdot 10^8$ is chosen, which a rather high value. This is chosen to only prevent the NLS method from diverging, which occur occasionally.

This covariance estimation have however shown to be rather optimistic and often leads to a too small estimated covariance. Thus it is instead used as an extension to (2.18), resulting in the new, augmented covariance matrix

$$P^a = \begin{bmatrix} P_{xx} & P_{xm} & (G_x P_{xx})^T \\ P_{mx} & P_{mm} & (G_x P_{xm})^T \\ G_x P_{xx} & G_x P_{xm} & G_x P_{xx} G_x^T + G_y R G_y^T + P^{NLS} \end{bmatrix}. \tag{3.36}$$

Choice of Parameters

Both the number of measurements used in the initialisation and the parallax threshold can be tuned for either a faster initialisation or more accurate landmark mapping. As seen in (3.30), the variance of the artificial range estimate depends on the parallax angle alpha, where a parallax angle close to 90° yields the lowest achievable variance while a parallax close to 0° makes the variance approach infinity. This is also illustrated in Figure 3.7.

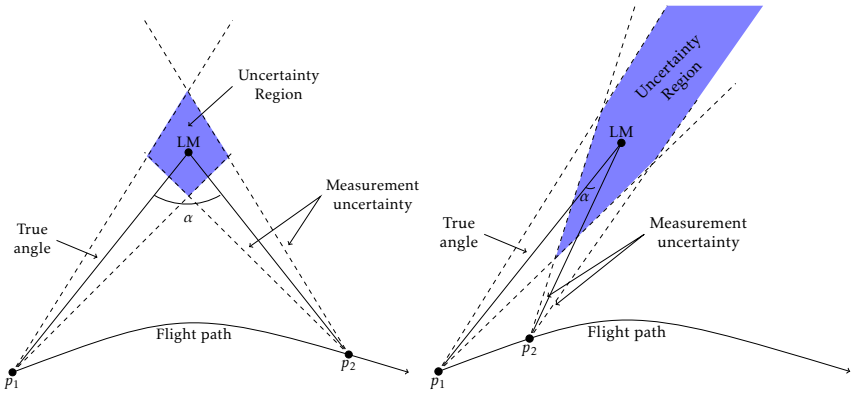

(a) *Large parallax angle.* ***(b)*** *Small parallax angle.*

Figure 3.7: *Illustration of how the estimation uncertainty varies with the parallax angle. A larger parallax yield a smaller uncertainty region while a parallax close to 0 ° may cause the uncertainty region to approach infinity.*

3.6 Aircraft Positioning with Known and Unknown Source Locations

As described above, two filters have been implemented, where one handles known signal sources and one handles unknown sources. However, in most realistic cases, the signals reaching the aircraft are a combination of known and unknown sources. To handle this, the known source locations are also added to the initial state vector with their known coordinates according to

$$\hat{z}_{1|0} = \begin{bmatrix} x_{1|0} \\ \mathbf{m}_{1|0} \end{bmatrix}, \tag{3.37}$$

where $x_{1|0}$ are initial values of the position and velocity of the aircraft and $\mathbf{m}_{1|0}$ are the initial known source locations. The initial covariance is defined as

$$P_{1|0} = \begin{bmatrix} P_{1|0}^{xx} & 0 \\ 0 & P_{1|0}^{mm} \end{bmatrix}, \tag{3.38}$$

where $P_{1|0}^{xx}$ is the initial covariance of the position and velocity of the aircraft and $P_{1|0}^{mm}$ is the covariance of the known source locations. Since the state is initialised with the true source locations, the covariance is initialised close to zero. The problem is then solved in the same way as described in Section 3.5.

4

Simulation Study

In this chapter, the models and methods used for state estimation presented in Chapter 2 and Chapter 3 are tested. The study aims to present the results needed to answer the questions investigated in this thesis. The performance of the estimators is evaluated through the achieved RMSE over time and ANEES for the estimated position and velocity states. Furthermore, the filter consistency is tested by analyses of the innovation. Also, the computational complexity of the filters are evaluated using time analysis.

4.1 Parameter Selection

This section aims to evaluate and choose standard parameters which are used in the rest of the simulation study.

4.1.1 Test Scenario

The standard test scenario in the simulation study can be seen in Figure 4.1a. A total of 6 sources is used in an area of 15 000 km^2 which gives a source density of $4 \cdot 10^{-4} \frac{sources}{km^2}$. The process noise covariance is set to $Q_k = 0.0283^2 \cdot I_{2\times 2}$, since it results in an average ANEES around 1 for the whole simulation, see Figure 4.1b. The fluctuation of the ANEES over time is likely caused by a combination of the shape of the trajectory and the simplified INS model used. The model assumes a constant velocity between the sampled points which means that the estimation error naturally should increase when the path is turning, meaning that the true velocity direction changes, compared to when the path is straight. The increased estimation error is not accounted for in the covariance update, since a fixed Q is used, and thus the ANEES value increases.

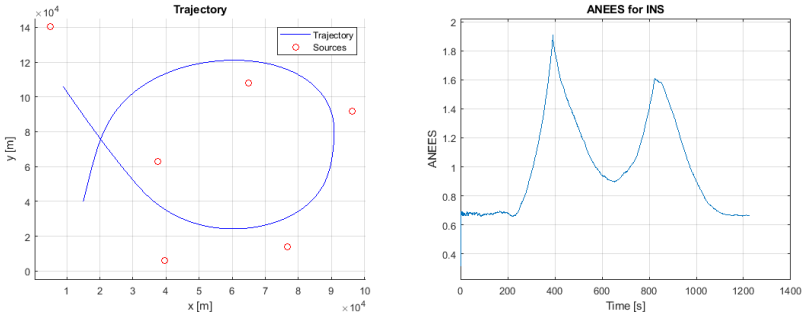

(a) Map and Trajectory for standard test scenario.

(b) ANEES of 1000 MC simulations for INS.

Figure 4.1: *Standard Test Scenario and ANEES for INS*

4.1.2 Measurement Characteristics

This section aims to evaluate how the DOA localisation is affected by different levels of measurement noise and different frequencies of the measurement update. These parameters are varied individually on the scenario described in Section 4.1.1 and the results are evaluated by comparing the RMSE over time for the case of all known as well as unknown sources using the EKF and EKF SLAM approach. The signal measurement error is assumed to be Gaussian distributed noise according to

$$e_k \sim \mathcal{N}(0, \sigma_e^2),$$

with equal variance $R_k = \sigma_e^2$ for all incoming signals.

In the first test, the magnitude of σ_e is varied in the range from 0.2 to 2° while all other parameters are held constant to see how the positioning performance is affected. The results can be seen in Figure 4.2a and Figure 4.2b. The RMSE is lower for all tested noise levels in both cases compared to the RMSE of the unassisted INS. However, a higher noise seems to increase the RMSE and lead to a slower convergence as well as more fluctuations. These characteristics does also seem to get more affected when using unknown sources compared to known sources.

When analysing the measurement update frequency, it is varied between 0.033 and 5 Hz while σ_e is kept constant at 1°. The lower frequency bound is set to the estimated frequency of weather radars and the higher bound is set to the time update frequency. The results can be seen in Figure 4.3a and Figure 4.3b. The RMSE is lower for all tested frequencies in both cases compared to the unassisted INS. Similarly as for increased noise, a decreased frequency seems to increase the RMSE, which leads to a slower stabilisation and larger fluctuations. Again, these characteristics are affected more when using unknown sources. Note that the RMSE has not yet stabilised for 0.033 Hz during the studied time in Figure 4.3b. It can also be seen that the RMSE difference decrease less when the frequency

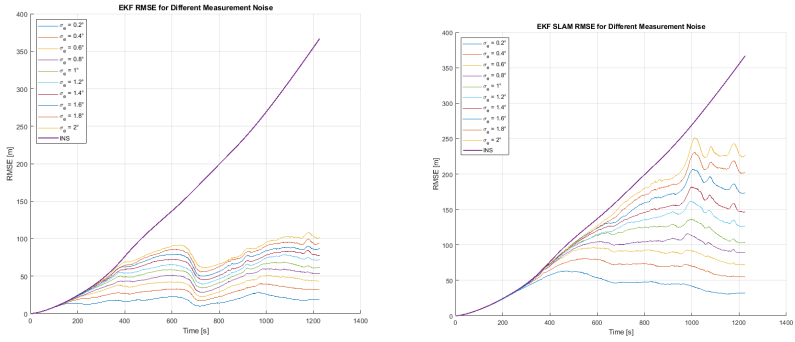

(a) Known source locations. *(b) Unknown source locations.*

Figure 4.2: *RMSE of 1000 MC simulations when varying the measure noise.*

approaches the maximum frequency of 5 Hz.

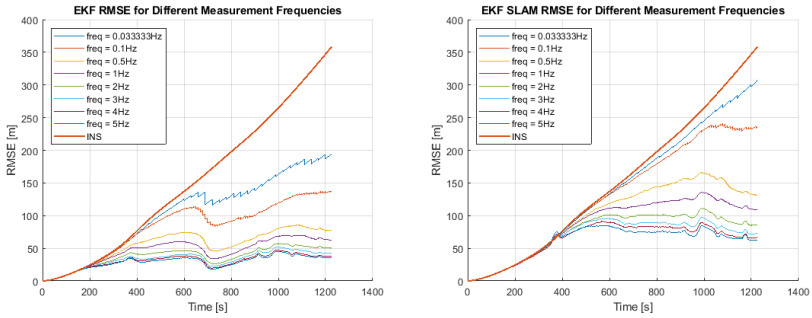

(a) Known source locations. *(b) Unknown source locations.*

Figure 4.3: *RMSE of 1000 MC simulations when varying the measurement update frequency.*

It is reasonable that the estimation error increase for lower measurement frequencies, since the INS is allowed to drift for a longer time before the measurements can correct the position estimate. This also leads to a less smooth path, as the position estimate needs to be corrected to a greater extent in the measurement update. This can be seen in the plot where the RMSE for low frequencies is much more sawtooth shaped compared to lower update frequencies. When the frequency is reduced, the INS drift has more influence on the RMSE and since the INS drift is not linear, the RMSE should not increase linearly when decreasing the frequency. This explains why the improvement in RMSE decreases as the measurement update frequency approaches 5 Hz.

The effects of increasing the measurement noise or decreasing the measurement frequency are more prominent when using unknown sources, which have several explanations. Firstly, a high noise might lead to a worse initial estimate of source position and covariance. A low frequency could also delay the initialisation since it takes a longer time to receive the needed amount of measurements. Even when the sources are initialised, noisy measurements can deform the map with each update and a lower frequency leads to less measurements available to lower the uncertainty of the sources.

4.1.3 Initialisation Parameters

Tests have shown that the performance of the SLAM algorithm is highly dependent on the quality of the landmark initialisation, as the filter requires that the estimated covariance of the landmark states correspond to the actual error in landmark position to work optimally. If the initial position error of a landmark is large but with a too small estimated covariance, there is a risk that the filter trusts the measurements too much which could interfere with both the aircraft position and the rest of the map states. If on the other hand, the covariance is estimated too high for a landmark, the measurements are not trusted even though they might be accurate, which reduces the benefit of utilising the landmark. The initialisation method presented in this thesis has been used to reduce the initial estimation error and provide a suitable initial covariance. As described in Section 3.5.2, the method can be tuned to achieve either faster or more accurate initialisation and this section aims to motivate the choice of these parameters.

Evaluations of different α_{th} and N_{meas} are seen in Figure 4.4a and Figure 4.4b, where tests are performed on a scenario similar to Figure 3.5. When evaluating α_{th}, the angle between p_1 and p_2 is increased by moving p_2 along a 10 km radius of a circle around a target m. When evaluating N_{meas}, the number of measurements is varied with fixed $\alpha_{th} = 30°$. The evaluation utilises CRLB for calculating the lowest achievable estimation error, as this value have shown to be similar to that of the NLS which is used in the initialisation process. The results show that the estimation error decreases, with an diminishing effect, when increasing the parallax angle and the number of measurements in N_{meas}.

The result from the parallax test is consistent with the theory described in Section 3.5, as a parallax close to 0° yields a very large estimation error and the value seems to be minimised when approaching 90°. However, while the performance significantly improves in the beginning, there does not seem to be any large difference between using a 30° parallax compared to 90°. One should also keep in mind that a fast initialisation is desirable, which is why a smaller parallax could be preferred. The test does however only show the result for when the magnitude of the measurement noise is set to 1°. If the noise were to be increased, a larger parallax angle would be needed, according to (3.30).

When analysing the estimation error as a function of the number of measure-

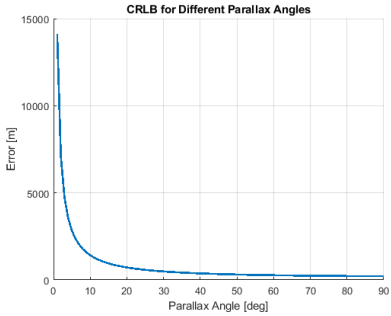

(a) Varying the parallax angle α.

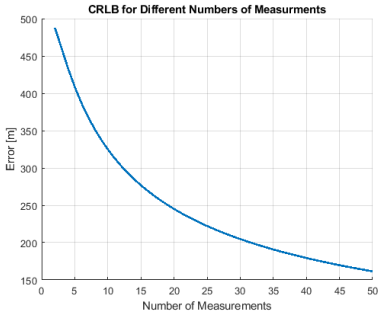

(b) Varying the number of measurements N_{meas}.

Figure 4.4: *Simple tests to evaluate different α and N_{meas}, conducted using CRLB. The scenario is set up in a similar way as in Figure 3.5.*

ments used, the results show that more measurements yields a lower estimation error. This is in accordance to the theory, as the CRLB depend on the FIM in (2.20), which increases with the number of observations provided. The plot indicates that the error keeps decreasing even after 50 measurements, but the test was limited to this value since storing more measurements was not considered reasonable given that both the computational power and memory capacity are limited resources on an aircraft.

4.1.4 Choice of Parameters

The RMSE characteristics seems to be similar for different noises and as the study aims to represent realistic results, a value in the middle of the spectrum is chosen. The same applies for the measurement frequency, where a too low frequency would not show the impact of the measurements too well and a too high frequency would decrease the purpose of using the time update from the INS. The INS is run at 5 Hz [3] in all simulations and the unassisted INS is used as a baseline for the evaluation of the performance. The initialisation tests show that the gain in performance is significantly reduced after a parallax around 30°. Increasing the number of measurements used in the initialisation do continue to improve the lower bound of the estimation error even for high values. However, as both computational complexity and memory usage are limited assets, a rather small value is chosen. The selected parameters are displayed in Table 4.1, and are used as default in further tests if nothing else is stated.

The initial states are assumed to be known at start and with initial covariance

[3] A real INS usually have an update frequency of 50+ Hz, but 5 Hz is used to save simulation time. This can be used since only the characteristics of the drift is used for comparison and it is tuned to achieve a similar drift as a real INS would have.

Table 4.1: *Selected parameters*

Parameter	Value
σ_e	1.0°
Measurement frequency	1 Hz
INS frequency	5 Hz
α_{th}	30°
N_{meas}	10
Monte Carlo runs	1000

according to

$$\hat{z}_{1|0} = \begin{bmatrix} x_{true} \\ \mathbf{m}_{true} \end{bmatrix}, \quad P_{1|0} = 10^{-6} \cdot \begin{bmatrix} 1 & 0 & 0 & 0 & 0 \\ 0 & 1 & 0 & 0 & 0 \\ 0 & 0 & 1 & 0 & 0 \\ 0 & 0 & 0 & 1 & 0 \\ 0 & 0 & 0 & 0 & I \end{bmatrix}, \tag{4.1}$$

where I is an identity matrix twice the size of the number of known sources and is used together with $\mathbf{m}_{true}$ when they are included in the state.

4.2 Scenario Evaluation

In this section, tests are conducted to investigate how the DOA localisation performance for known signal source locations is affected by the number of available signal sources and how they are distributed in the surrounding environment. Here, all signals are assumed to arrive simultaneously and none of the signals have limitations regarding their range. Furthermore, tests are conducted to see how the SLAM performance is affected by the flight trajectory when using sources with unknown location.

4.2.1 CRLB for Known Sources

The tested scenarios are divided into two categories depicted as a land scenario and a coast scenario. All tests are conducted using 100 Monte Carlo simulations for each density by resampling the map each iteration. Initial set-up evaluations are conducted with heatmaps where the lower bound of the estimation error according to CRLB is calculated for each point on a grid in the investigated map set-up. The scenarios are also evaluated with the parametric CRLB for a filter approach, as described in Section 2.4.2, for a given trajectory. For the land scenario, the signal sources are assumed to have a uniform, random distribution with a certain density which is varied between $1 \cdot 10^{-4}$ and $1 \cdot 10^{-3} \frac{sources}{km^2}$ in the tests. To simulate a flight along the coast, all signal sources are placed on one side of the flight path. Again, the number of sources are varied, but also the distance to the

coast. The different scenarios and the result of the parametric CRLB are shown in Figure 4.5.

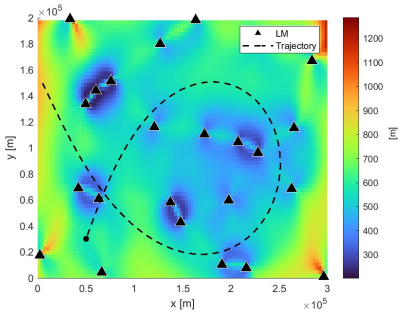

(a) CRLB heatmap land scenario.

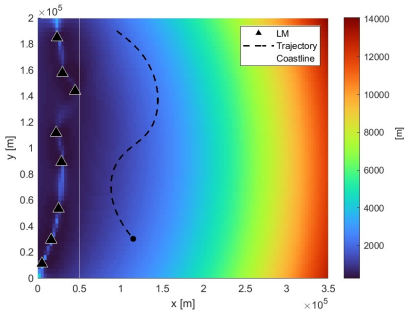

(b) CRLB heatmap coast scenario.

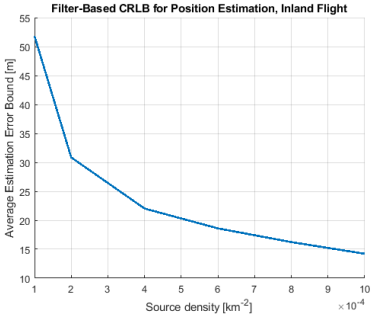

(c) Filter CRLB land.

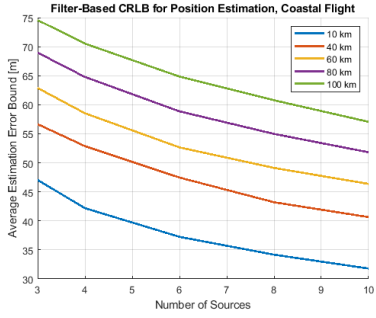

(d) Filter CRLB coast.

Figure 4.5: *Top: Examples of the different test set-ups with a heatmap depicting the size of the non-filter CRLB of the estimation error in different parts of the map. Bottom: Lower bound of the estimation error according to CRLB. The plot shows an average calculated for the entire trajectory and for 100 MC runs where the map have been resampled each iteration.*

The heatmaps indicate that positioning using DOA measurements gives a fairly even estimation error while flying inland with uniformly distributed landmarks. The estimation error seems to increase when flying along the coast as the distance to shore is increased, which is reasonable as the uncertainty region from each measurement should grow with the increased distance. Furthermore, the heatmap indicates that the estimation error should increase when flying straight in between two landmarks. This is also intuitive, as the measurements from both signal sources only give information that the aircraft is somewhere on an line in between the sources, and additional measurements are required to be able to pinpoint the location along the line. Thus, in a scenario where only one signal source is available or when passing through sources with the same LOS, the localisation

uncertainty approaches infinity and a location can not be determined using only DOA measurements. Since the heatmap is based on a non-filter CRLB approach, the calculated values for the lower bound of the estimation error are higher than the estimation errors achieved when using a filter. Thus, the numerical values presented in the heatmaps are only used as an indicator of the DOA localisation performance.

The results of the parametric CRLB for the trajectory show that the estimation error seems to decrease, with a diminishing effect, when the source density is increased. This indicates that even though an increased number of sources decreases the estimation error, the benefits of utilising more sources at the same time becomes less significant for higher densities. The result is reasonable since increasing the number of measurements increases the Fisher information which reduces the CRLB. This is also consistent with the results from the heatmaps, as an increased amount of randomly placed sources decreases the number of uncertain regions in between sources. The effect is probably less prominent for higher densities, as when many sources are available, the level of uncertainty is rather even throughout the map and adding an additional source does not make a big difference. Also, a higher density increases the probability that signals have similar DOA, and are thus removed according to (3.3).

The coastal scenario show similar results with decreasing estimation error with an increase in number of sources, and a fairly linear relationship between the distance to the coast and the lower bound of the estimation error, which can also be seen in the coastal heatmap. The estimation error is not significantly increased for the coastal scenario compared to the land scenario. This is probably because the coast is wide with evenly spread sources compared to the distance to the aircraft, which means that the angle difference between the measurements from sources in the top and the bottom of the map is still large enough to limit the uncertainty region of the aircraft. The results from the filter CRLB indicate that the best localisation accuracy when using DOA from known signal sources should be in the range of 10 to 100 meters at this scale. This could be considered an acceptable accuracy given the scale of the problem, even though it does not match the accuracy of GNSS.

4.2.2 Flight Trajectory Evaluation for SLAM

This section aims to compare the EKF SLAM algorithm performance for when flying straight through an environment and for when staying a longer time in the same environment, according to Figure 4.6. This is done to investigate how the trajectory affect the DOA localisation when using sources with unknown locations. In this test case, a land scenario is used with a source density of $2 \cdot 10^{-4} \frac{sources}{km^2}$ and the signal sources are placed equally in both tests.

In Figure 4.7, it becomes clear that the unknown sources do not provide any improving effect for the localisation performance in the case where the aircraft

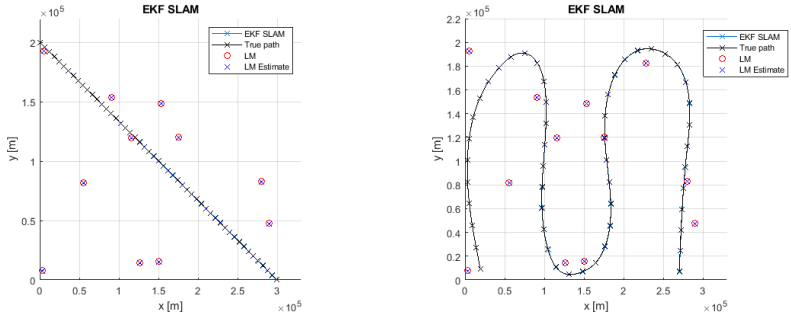

(a) Straight fly-fhrough. *(b) Winding flight path.*

Figure 4.6: *Different estimated flight trajectories using EKF SLAM in the same test environment.*

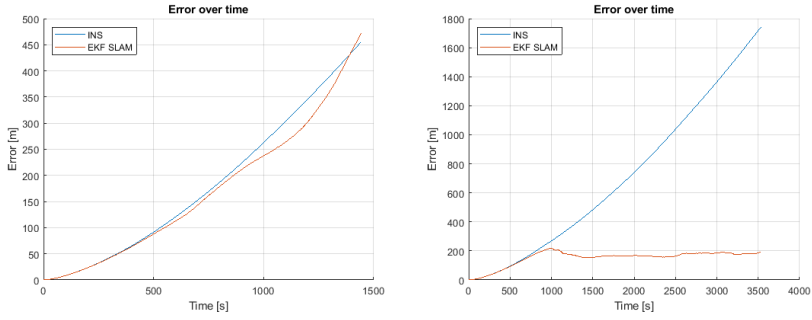

(a) Straight fly-through. *(b) Winding flight path.*

Figure 4.7: *RMSE for the aircraft position over time for two flight paths in the same environment.*

quickly passes through the environment, while the other case show significantly lower RMSE than the INS. When investigating the landmark position error in Figure 4.8, one can see that for the case with the straight path, the landmarks are initialised late relative to the total simulation time and their absolute error have not settled until the end of the run. Thus, the aircraft has passed through the environment before it could utilise the mapped landmarks for localisation. When circulating the environment, the effect of using the unknown sources becomes prominent, as the filter has had time to properly map the landmarks and their estimated covariance have become low enough to affect the state estimate of the aircraft.

These tests indicate that the choice of flight trajectory is an important factor for the SLAM algorithm, since the time spent in a certain environment has great in-

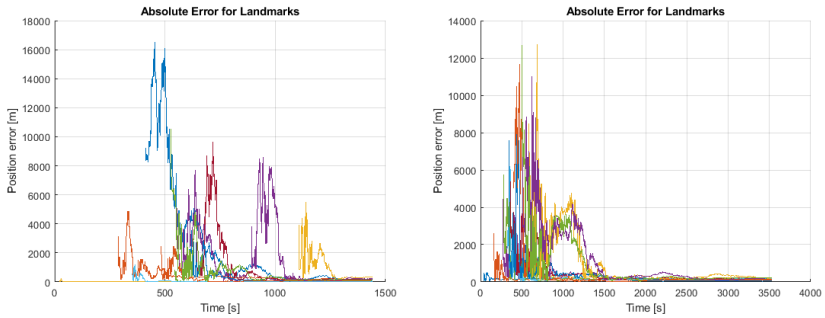

(a) Straight fly-through. *(b) Winding flight path.*

Figure 4.8: *RMSE for the landmark positions over time for two flight paths in the same environment. Each color represents the absolute error for one landmark.*

fluence on the localisation performance. For unknown signal sources, the SLAM algorithm needs to observe landmarks, initialise them into the filter and then reduce their estimated covariance before they can be used for positioning of the vehicle itself. This process takes time, and thus, less time is left to utilise the sources for navigation when passing through several landmarks fast. In these cases, it might be beneficial to lower the parallax threshold so that landmarks are initialised at an earlier stage and thus have more time to improve the navigation performance. Reducing the parallax threshold does however increase the risk of badly initialised landmarks which might affect the localisation negatively. A similar effect can be achieved if the aircraft speed is reduced or if the measurement update frequency is increased, as the landmark state estimation is highly dependent on the amount of observations that is provided to the filter. However, this does not decrease the initialisation time. Given this, a flexible solution for the initialisation method might be useful.

Given these results, the standard case in Figure 4.1a used in the other tests have been selected so that the DOA based positioning performance is fairly equal throughout the map and with a path that allows the aircraft to stay a longer time in the same area.

4.3 Outlier Rejection

This section provides an analysis of the robustness against measurement outliers in the filters as well as an evaluation of the filter consistency. This is done by using both measurements with and without added outliers, as a reference [4]. The simula-

[4]The measurements used to initiate landmarks in the EKF SLAM approach do not include outliers. This is done since a landmark position estimate is needed for (3.8) to work and to make sure that the results only depend on how well the filters handle outliers. A separate analysis on how the landmark

tions are performed on the scenario described in Section 4.1.1 using known and unknown sources with EKF and EKF SLAM. The robustness against the added outliers is evaluated using the RMSE of the aircraft position and the filter consistency is evaluated using ANEES and with an evaluation of the innovation. The difference between using $p_O = 90\%$ and $p_O = 99\%$ is also evaluated.

The outliers are generated using a matrix with additional noise, $e_O \sim \mathcal{N}(0, \sigma_O^2)$, where $\sigma_O = 15°$, in the same size as the generated DOA measurement samples. The samples where

$$|e_O| < 3\sigma_O, \tag{4.2}$$

is fulfilled are then set to 0, since outliers are only wanted on a small fraction of the measurements. This matrix is then added to the DOA measurement matrix. This means that the added outliers are angles of at least 45° which are distributed over 0.3% of the DOA measurement samples.

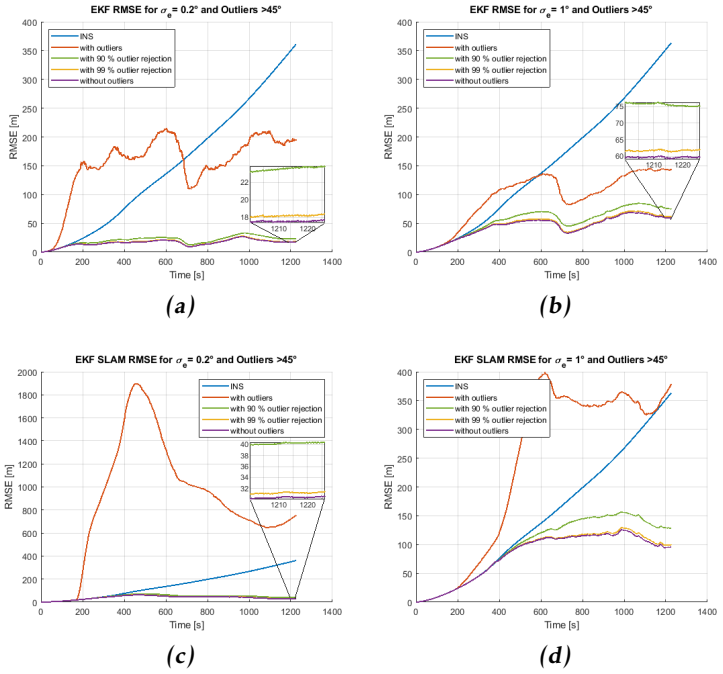

Figure 4.9: *RMSE when outliers are added. An EKF is used for known sources and EKF SLAM for unknown sources. The RMSE when no outliers are added acts as a reference.*

When evaluating the RMSE in Figure 4.9, one can see that it is much higher if no rejection is used, and that the system is even more sensitive to outliers when

initiation handles outliers is presented in Section 4.4.

a lower noise is investigated, especially when using unknown sources. In this scenario, $p_O = 99\%$ seems to be a better setting since the RMSE is lower than for $p_O = 90\%$ in all cases. This is even more obvious when the measurement noise is higher. In fact, almost no visible difference can be seen when comparing the RMSE using $p_O = 99\%$ and the reference without any added outliers. In Figure 4.10 the ANEES after outlier rejection looks similar to that of the INS while the ANEES if no rejection is used is higher, especially when using unknown sources. In Figure 4.11, the ANIS is close to 1 when rejection is used and much higher when no rejection is used. The difference between EKF and EKF SLAM in this case is that there are higher spikes in the ANIS for the EKF SLAM. In Figure 4.12, the histograms look Gaussian with zero mean both when using rejection and when no outliers are added. When no rejection is used, the innovation has zero mean but is less Gaussian due to more values in the tails of the histogram caused by the outliers. The same result is obtained when using unknown sources, but with a slightly higher variance of the innovation when no rejection is used.

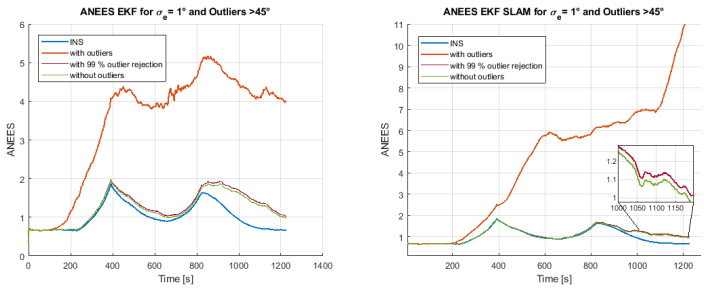

Figure 4.10: *ANEES over time. An EKF is used when all sources are known and EKF SLAM is used when the sources are unknown. The ANEES for INS is used as a reference and have an average of 1 over time.*

The results indicate that the used outlier rejection improves the filter robustness against outliers. Even though the results show that outlier rejection is important in all cases, they also show that the error is more affected when the measurement noise is lower and that outlier rejection is extra important in those cases. This is reasonable since R_k in the filter is equal to the actual measurement variance that is added to the simulated measurements. This means that if the filter is tuned for a low noise variance, the added outliers become relatively bigger compared to when a higher variance is expected. It is also reasonable that the EKF SLAM approach is more affected by outliers since each time an outlier is used, the map slightly changes. In the EKF approach, the map is stationary meaning that only the aircraft position is affected.

Furthermore, a high ANEES which is the case without outlier rejection would

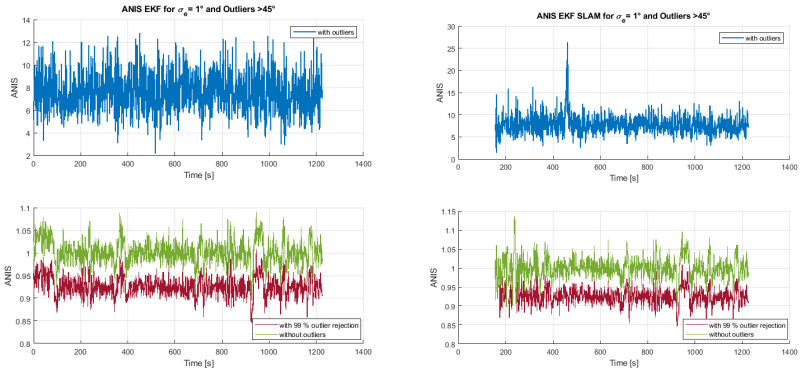

(a) *(b)*

Figure 4.11: *Evaluation of innovation using ANIS. An EKF is used when all sources are known and EKF SLAM is used when the sources are unknown. The ANIS achieved without added outliers is used as a reference.*

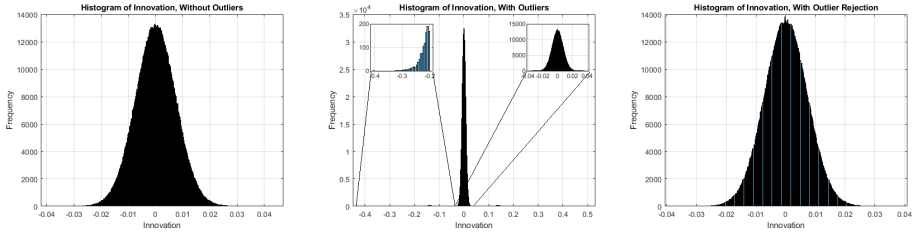

(a) *(b)* *(c)*

Figure 4.12: *Evaluation of innovation using histograms when known sources are used.*

mean that the estimated covariance is too low. This is bad since it indicates that the position estimate is more certain than it actually is. This is reasonable since the filter covariance R_k is constant and can thus not compensate for unexpected deviations. With this said, the achieved ANEES has an average slightly above 1 indicating a somewhat optimistic estimated covariance. However, the spikes causing a higher ANEES for the filter can also be seen for the unassisted INS and is probably caused by model error in the INS. Though, compared to when no rejection is used, the results are significantly improved and the filters are more trustworthy. The ANIS after the outlier rejection is slightly below 1, indicating a decent but somewhat high estimated innovation covariance. This could be caused by the outlier rejection removing enough measurements to lower the variance. The innovation analysis resulted in a Gaussian distribution with zero mean when outlier rejection is used. This together with a decent ANIS and ANEES indicate

filter consistency which is important for robustness. This does not seem to be true without outlier rejection.

4.4 Landmark Initialisation Method

This section aims to evaluate the robustness against outliers in measurements used for initialisation and to test how the DOA performance is affected by the choice of initialisation method. This is performed by testing the performance of the NLS extension in the initialisation process, as described in Section 3.5, and compare against when only the artificial range-bearing method is used to initialise the landmark directly. These two methods will be referred to as NLS method and artificial measurements (AM) method respectively. The tests are conducted using the same setup as in previous tests and are divided into two parts. The first test is constructed to evaluate how the two methods perform when outliers are manually added to the initial observation of each of the landmarks. In this test, the number of measurements used in the NLS method N_{meas}, is also varied. The second test aims to compare the DOA performance for the two methods when the measurement noise is varied.

4.4.1 Robustness Test with Added Outliers

The resulting RMSE for the aircraft position at different level of manually added outliers can be seen in Figure 4.13. In Figure 4.14, the ANEES for the full map state have been plotted over time.

The plots show that the RMSE go towards lower values when using the NLS method than the AM method, in all cases. The value of N_{meas} does not seem to affect the RMSE much for 10° added outliers, but does so for 20° outliers. In this case, more measurements seem to have a positive effect on the performance. The ANEES plots for the map state shows that an increased number of NLS measurements tend to lead to an ANEES approaching 1. This is seen in Figure 4.14a, where $N_{meas} = 50$ is the only setting with an ANEES close to 1 throughout the whole simulation. The ANEES when only using the AM method diverges to extremely high values, indicating that the estimated covariance is substantially smaller than the actual position estimation error. An example of this can be seen in Figure 4.15, where one can see that the estimation and covariance is much less accurate for the AM method than for the NLS method.

When greater outliers are added, such as in Figure 4.13c, the AM estimate have an error very close to the INS through the simulation. An explanation for this can be found by analysing the estimated path and mapped landmarks for the different methods, as seen in Figure 4.16. It becomes evident that the landmarks for the AM method have been estimated at the completely wrong location, with small estimated covariances. This is likely caused by the 30° initialisation threshold being equal to the added outlier. When investigating the number of measurements

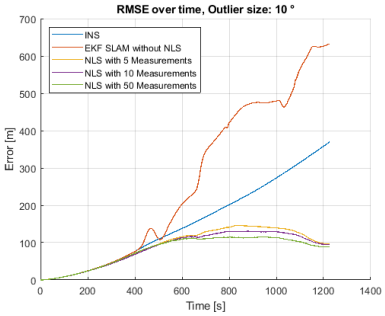

(a) RMSE plot for Outlier magnitude = 10°.

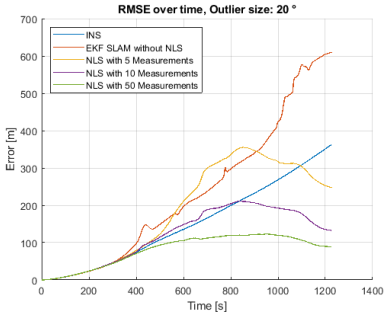

(b) RMSE plot for Outlier magnitude = 20°.

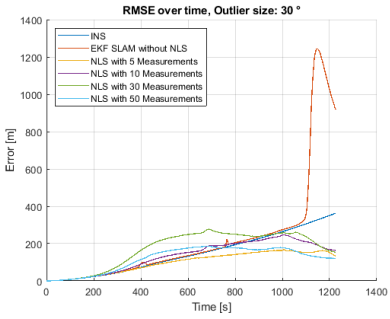

(c) RMSE plot for Outlier magnitude = 30°.

Figure 4.13: *RMSE of the position estimate for different initialisation methods, with added outliers in the initial values.*

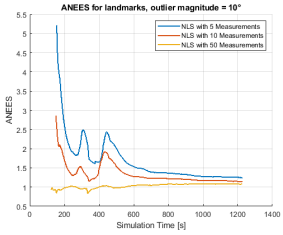

(a) Outlier magnitude = 10°.

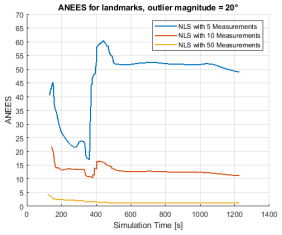

(b) Outlier magnitude = 20°.

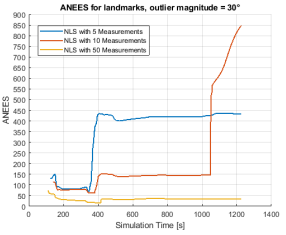

(c) Outlier magnitude = 30°.

Figure 4.14: *ANEES over time for the full map state*

that were used in the specific scenario displayed in Figure 4.16a, almost all measurements are rejected which explains why the position RMSE is almost identical

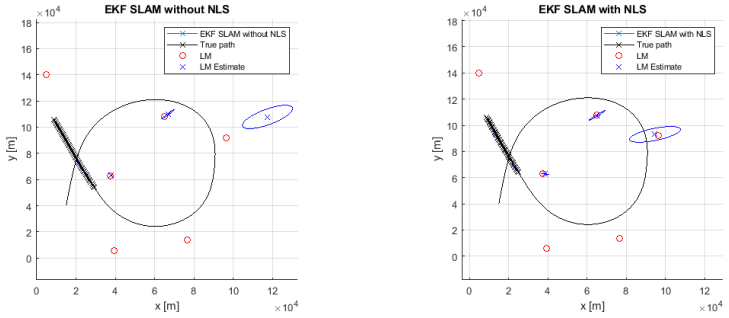

(a) AM method. *(b) NLS method.*

Figure 4.15: *Comparison of initial landmark position estimate for the NLS and AM methods when an outlier of 10° have been added to one of the measurements used in the initialisation. In both cases confidence regions with a 99% confidence level for the estimated covariance have been plotted. The black markers on the path indicate how far the aircraft has travelled at the time of initialisation.*

to that of the INS. This happens because the landmark estimates are completely wrong, causing a large innovation with a too small estimated covariance, which activates the outlier rejection. Therefore, the landmark estimate can not be corrected during the flight. In the end of the path in Figure 4.13c, the estimation error spikes. A measurement has therefore probably gotten past the outlier rejection since the estimated position is in a similar line of sight from the path as the true position.

The same type of behaviour have most certainly affected the results of the NLS method as well which is seen when investigating the absolute error of the landmarks in Figure 4.17. Here, landmarks that have been initialised with a very large initial error are not notably corrected during the simulation. This can also be seen in Figure 4.16, where the final position estimates are notably better when 50 NLS measurements are used instead of 5 NLS measurements. One can also see that the initial guess improves with the number of NLS measurements. This increases the probability that the expected measurements are similar to the actual measurements, implying that measurements from more landmarks are used. But, as seen in Figure 4.14c for 50 NLS measurements, the ANEES is still high, indicating a too optimistic covariance. This probably explains why the aircraft position RMSE for the different initialisation methods does not show the same correlations as when smaller outliers were added.

These tests have shown that the NLS method show significant improvements to the robustness against outliers during the initialisation and that the initial estimation error is reduced with the number of measurements used. However, when the

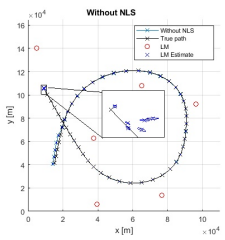

(a) AM method.

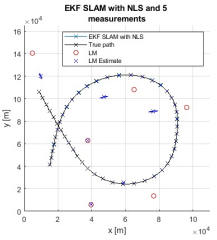

(b) NLS with 5 measurements.

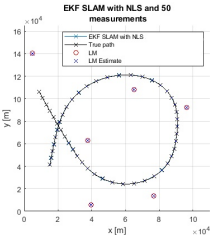

(c) NLS with 50 measurements.

Figure 4.16: *Estimated path and map for the AM method and different numbers of measurements used in the NLS when the initial measurement have been corrupted by a 30° error.*

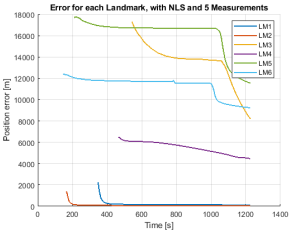

(a) NLS with 5 measurements.

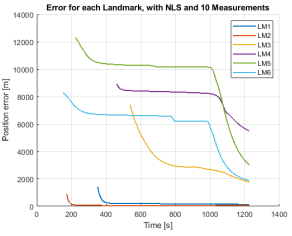

(b) NLS with 10 measurements.

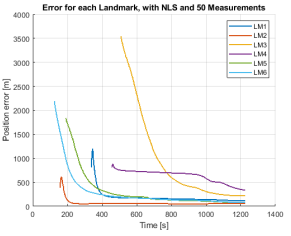

(c) NLS with 50 measurements.

Figure 4.17: *Estimation error of the landmark positions for different numbers of measurements used in the NLS when the initial measurement have been corrupted by a 30° error.*

measurement outliers are too large, the initial guess can become too poor, even when the NLS method is used. This either leads to a bad aircraft position estimate because of an optimistic covariance or triggers the outlier rejection and thus removes measurements. Therefore, the implemented outlier rejection method is not adapted for handling these types of large position errors, and another method would be necessary to fully compensate for bad initialisation performance before measurements are removed. One possible way of getting around the problem could be to utilise a second filter where the landmark positions and covariances are estimated before initialisation. The landmarks are then only included in the main filter if their estimated covariances are low enough.

4.4.2 Initialisation for Different Magnitude of Measurement Noise

When varying the measurement noise, tests are conducted with $\sigma_e = 1°$ and $\sigma_e = 2°$, and $N_{meas} = 10$. The resulting RMSE is displayed in Figure 4.18. In Figure 4.19, the RMSE for each initialised landmark have been plotted over time for when the noise magnitude is set to 2°.

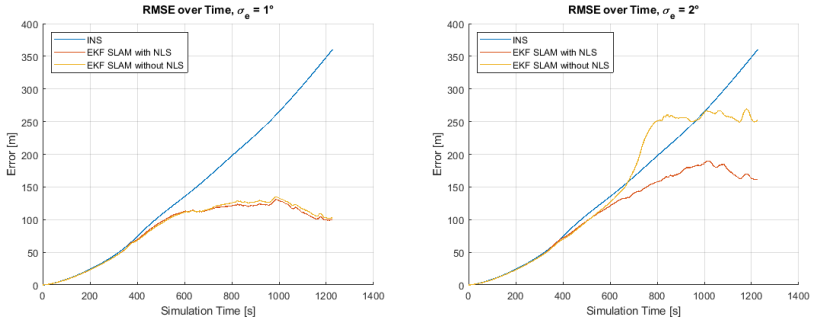

(a) RMSE plot for $\sigma_e = 1°$. *(b) RMSE plot for $\sigma_e = 2°$.*

Figure 4.18: *Comparison of aircraft position RMSE with and without NLS in the initialisation.*

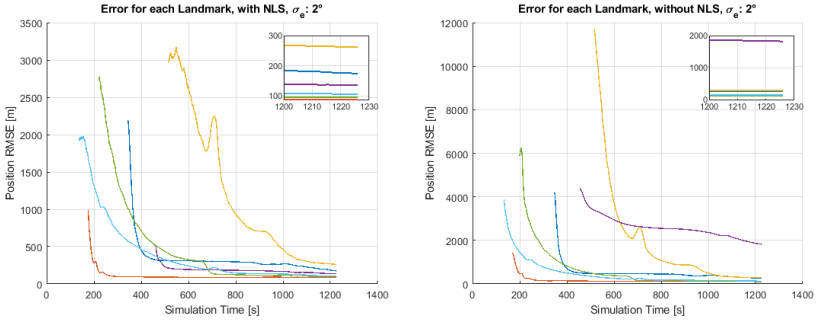

(a) RMSE for the landmark positions using NLS initialisation. *(b) RMSE for the landmark positions using AM method.*

Figure 4.19: *Comparison of landmark position RMSE with and without NLS in the initialisation for $\sigma_e = 2°$.*

The results indicate that the positive effects of using the NLS method are small when $\sigma_e = 1°$, but become more evident when $\sigma_e = 2°$, since the final RMSE is about 100 meters higher without the NLS extension. This indicates that a robust initialisation method is an important process to achieve a better DOA localisation. This can also be seen in Figure 4.19, where there are significant improvements in

the initial estimated landmark positions when using the NLS method. One can also see that the position error quickly drops to fairly low values. For the AM method however, one of the landmark continues to have a significant position error at the end of the simulation. This is probably the result of a too small estimated covariance or bad initialisation which, as discussed earlier, activates the outlier rejection. Furthermore, the ANEES for the full state of the landmark positions resulted in very high values, reaching 350 in the end, indicating a too low estimated covariance. In comparison, the ANEES for the NLS approach stays around 1 for the entire simulation.

4.5 Combining Known and Unknown Sources

This section provides an analysis on the advantages of utilising a combination of sources with known and unknown locations. The test scenario can be seen in Figure 4.20, where known sources have been placed with a density of $2 \cdot 10^{-4}$ $\frac{sources}{km^2}$ and unknown sources with a density of $6 \cdot 10^{-4}$ $\frac{sources}{km^2}$. A higher density of sources with unknown locations is chosen since this is probably true in realistic scenarios. The position is estimated using EKF SLAM and known sources are added to the filter using the approach described in Section 3.6. This scenario is analysed using three different cases. One where only the known sources in Figure 4.20 are used, one where both known and unknown sources are used and one where all 16 sources are classified as unknown. The measurement frequency as well as the measurement noise is altered to see how the performance is affected.

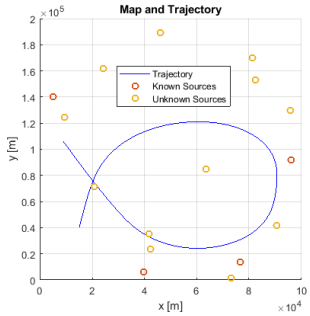

Figure 4.20: *Trajectory and map with known and unknown sources.*

In Figure 4.21a, it can be seen that only using known sources at a frequency of 0.03 Hz seems to only slightly increase the performance compared to the INS. There also only a slight difference between the combination and when all sources are unknown, indicating that using known sources with a low measurement frequency does not show significant advantages compared to when all are unknown. A higher frequency of either known or unknown signals results in a more constant RMSE over time. This can be seen in Figure 4.21b where the frequency of

known sources is increased to 1 Hz. This indicates that the advantages of utilising a combination of sources become more prominent when they can be used with a higher measurement frequency. Finally, the results show that in this scenario, the final RMSE value of only unknown sources is at least as good as the RMSE achieved when using only known sources in all cases. This is likely because there are 4 times more unknown than known sources and when they have decent estimation, a higher accuracy can be achieved.

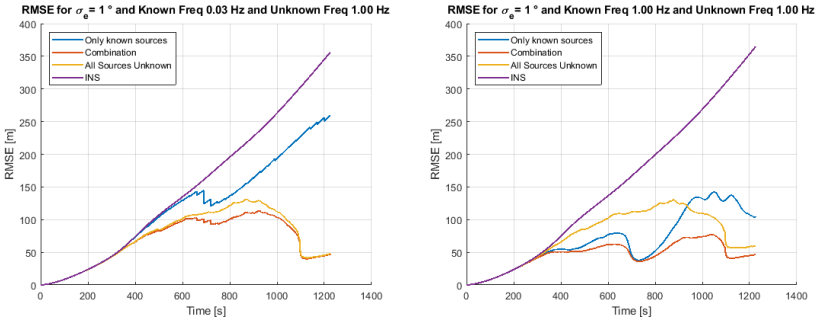

(a) *(b)*

Figure 4.21: *RMSE when varying the measurement update frequency for only known sources, a combination of known and unknown sources and for only unknown sources.*

In Figure 4.22a, when a lower measurement noise is evaluated, the combination still gives the best performance, although the difference is less significant. On the contrary, when increasing the noise as in Figure 4.22b, a more fluctuating RMSE with higher peaks is achieved for all cases. The difference in RMSE between the combination and the other cases individually also becomes larger, showing the advantages of using a combination of sources.

The results indicate that the advantages of using a combination of sources depends on what measurement frequency they can be updated with. With a higher frequency, the known sources can be used to get an absolute position, which is especially important before the unknown sources have converged to a decent estimate. This behaviour can be clearly seen in Figure 4.21b, where the RMSE stays around the same value throughout the simulation even though the RMSE for the two other cases fluctuates significantly during the simulation. This indicates that when utilising a combination, the performance always seems to be better than the two other cases individually. The behaviour seems to remain the same regardless of the measurement noise. Although, the effect of utilising known sources seems to be more valuable if the measurement noise is high, as the accuracy of the initial estimates of unknown source have been proven to correlate with the level of noise. However, in this case the aircraft remains in the area a longer time, giv-

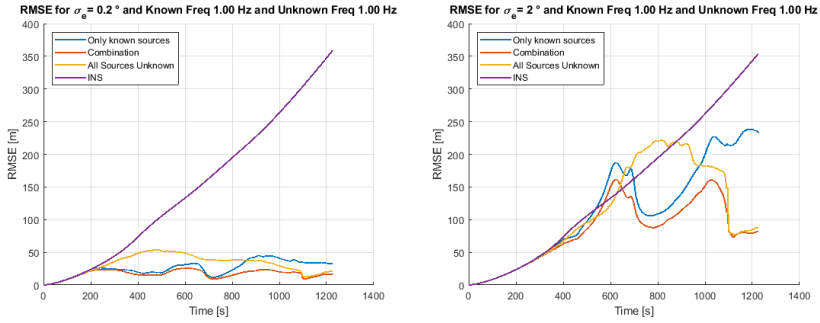

(a) *(b)*

Figure 4.22: *RMSE when varying the measurement noise for only known sources, a combination of known and unknown sources and for only unknown sources.*

ing the EKF SLAM enough time to get a decent estimate of the unknown sources. If instead a trajectory more similar to the one in Figure 4.6a would have been used, the result when only using unknown sources would probably be worse. Therefore, by having some known sources, the absolute aircraft position could be maintained since the estimate does not drift as much as it would with an unassisted INS. This would also improve the estimates of the unknown sources since they depend on the aircraft position.

Furthermore, to get an even better understanding of the advantages of known sources, future tests could investigate how the performance is affected when the ratio between unknown and known sources is altered but the total number of sources is fixed. It would for example be interesting to investigate how the unknown source estimates are affected when increasing the number of known sources.

4.6 Realistic Flight

In this section, the overall performance of two longer, more realistic scenarios is tested, where the signal sources are a mixture of known and unknown sources. An analysis of the filter consistency is also provided. The sources are roughly based on the different types described in Section 3.2 and are divided into 4 categories. The sources are categorised as weather radars, 4G cellular towers, mixed known radars and mixed unknown radars and their definitions are presented in Table 4.2. The characteristics of these types differ as they have different signal range, signal rate and are spread with different densities over the map. The mixed sources aim to represent the vast range of different types of civilian and military radars. The availability of sources with unknown locations are assumed

to be significantly higher than sources with known locations.

Table 4.2: *Traits of the different source categories used in realistic test flight.*

Type	Signal Range	Signal Rate	Density
Weather Radars	250 km	0.033 Hz	$1 \cdot 10^{-4}$
4G Towers	16 km	1 Hz	$1.2 \cdot 10^{-3}$
Unknown Mix	100 km	1 Hz	$4 \cdot 10^{-4}$
Known Mix	100 km	1 Hz	$1 \cdot 10^{-4}$

Furthermore, the performance is evaluated for when using only the known signal sources, using a combination of all available sources, and when assuming that all sources are unknown. This is done to see if the results are consistent with the results in Section 4.5.

4.6.1 Scenario Descriptions

The tested flight paths and source maps for the two scenarios are shown in Figure 4.23. The first scenario is constructed to replicate a flight where the aircraft is starting over land, then flies over the sea and then back to land.

The second test differs from the first as the aircraft returns to its starting position at the end of the run, and the map has a region in which only unknown sources are available. This is done to see if the results are consistent with the results in Section 4.2.2.

The process noise is tuned to $Q_k = 0.0231^2 \cdot I_{2\times 2}$ for both scenarios.

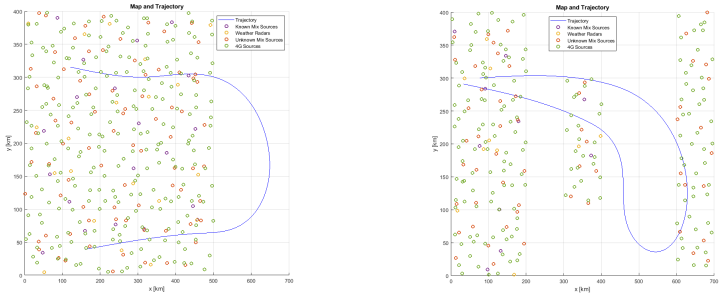

(a) *Scenario 1.* ***(b)*** *Scenario 2.*

Figure 4.23: *Test set-up for realistic scenarios. Here, different types of sources have been distributed with various characteristics and are plotted with different colors.*

4.6.2 Simulation Results

The results of the first realistic scenario can be seen in Figure 4.24a, where the RMSE of the aircraft position estimate is plotted over time for the different cases. Also, the parametric CRLB for the trajectory when only utilising known sources is plotted in order to evaluate the filter performance. The plot shows that all cases outperform the unassisted INS over time, although the case when known sources are used perform significantly better than when only unknown sources are utilised. The position error drifts for all cases in the middle of the simulation. Here, only some of the weather radars with a range of 250 km can be used for navigation, and these signals arrive with a very low rate, causing the estimate to drift with the INS between the measurement updates. However, when returning back to land, the position error drops to its previous values of about 100 meters when utilising known sources. This indicates that an absolute position can be found again even though the estimate has drifted during a period. The rate of drift seems to be approximately the same for the case with unknown signals. When the aircraft returns to land, the error seems to stop drifting and stabilises at a high position error of 1000 meters. Moreover, the RMSE for the case with only known source locations is close to the lower bound according to the parametric CRLB for the trajectory, with some exceptions.

In the second realistic scenario, the RMSE for when only the known sources are used is higher but has similar characteristics as in the first scenario, as seen in Figure 4.24b. The main performance difference can be seen when all sources are assumed to be unknown, as the RMSE does not stabilise at a high value as in the first test but instead drops down to the same low levels of around 100 meters as when when using known sources. Also, the combination of known and unknown sources show greater improvements in this scenario, as the error drift is reduced at $t = 2500$ compared to when no unknown sources are used.

In Figure 4.25, the resulting flight path estimate is shown together with the mapped landmarks for the cases where both known and unknown sources are used. Here, one can see how the SLAM algorithm has estimated the landmark positions and estimated a covariance, which can be seen as covariance ellipses.

In the first scenario, the error does not drop down to the same low levels as when using known sources, as the SLAM algorithm can only relate the mapped landmarks to its own estimated position. The error in the aircraft position causes all new landmarks to be initialised with a certain offset from their actual position, which distorts the map. This means that while the algorithm has no way of finding back to the absolute position of the aircraft and thus decrease the error, as for the case with known sources, the relative position to the landmarks is enough to cause the error to stop drifting.

In the second scenario however, the aircraft takes a more similar path back to the starting point, passing through environments that have already been discovered

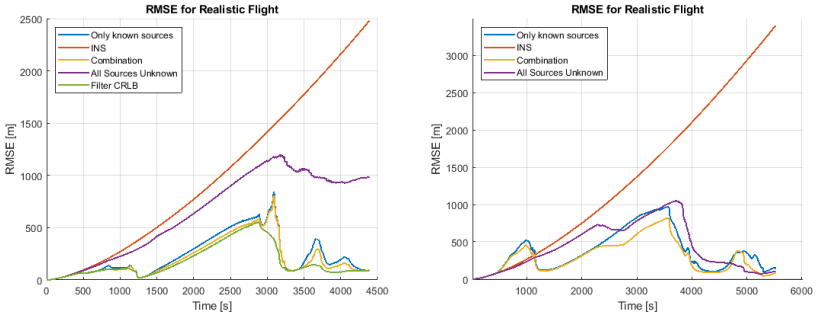

(a) Scenario 1. *(b) Scenario 2.*

Figure 4.24: *RMSE over time for the position estimates from the tested scenarios and compared to the unassisted INS. For the first scenario, the parametric CRLB for the trajectory is plotted as a reference.*

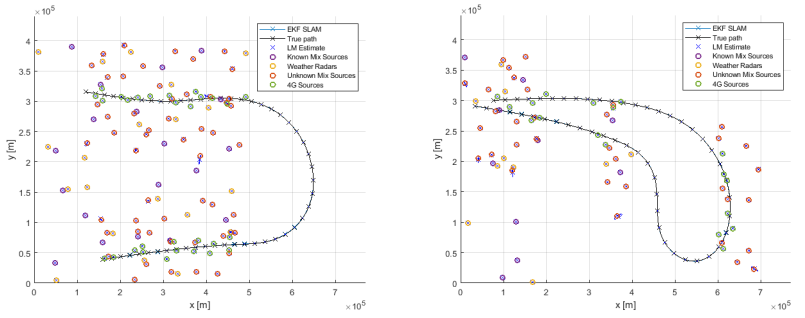

(a) Scenario 1. *(b) Scenario 2.*

Figure 4.25: *Estimated map and trajectory for realistic flights where a combination of known and unknown sources have been used. All visible sources have been added to the map of the SLAM algorithm.*

and mapped. When entering these previously visited areas, the RMSE of the position quickly drops and the error in the final position is even lower than when using only known sources. This shows promising results for the method to work even in completely unknown environments, although, one could achieve almost the same performance when using only a few known sources.

One can see that the overall performance for both scenarios is quite poor for a large part of the simulation, with estimation errors rising to several hundreds of meters in all cases. This is however caused by the long flight path where the DOA signals are few and arrive at a low rate, and as seen in the first scenario, the RMSE of the case with only known source locations is close to the lower bound

stated by the parametric CRLB. This indicates that the filter performance is close to the best achievable estimation error, while the SOO-DOA method is not very suited for longer flights over open sea where the source availability is low. However, there are some spikes in the RMSE which are not present in the parametric CRLB and indicates that the estimated covariance does not match the actual error at all times. Similar spikes can be seen for the second scenario, which is further discussed when analysing the filter consistency. Furthermore, utilising a combination of sources with known and unknown locations could improve and stabilise the performance compared to using either separately. For known source locations, the achieved RMSE is generally lower and an absolute position can be reestablished, but the number of available SOO could be limited as the method requires a database with stored locations. The availability of sources with previously unknown locations is likely much higher, which yields a more uniform signal coverage throughout environments where sources with known locations are sparse. All cases do however outperform the unassisted INS and the estimation error when flying over land is kept around 100 meters when using known sources.

4.6.3 Filter Consistency Results

For the second realistic scenario, some tests were also conducted to test the consistency of the EKF filter. In Figure 4.26, the 4D state ANEES for the aircraft as well as the ANIS for the filter have been plotted throughout the simulation. Also, the mean and variance of the innovation in the different cases are investigated using histograms as displayed in Figure 4.27.

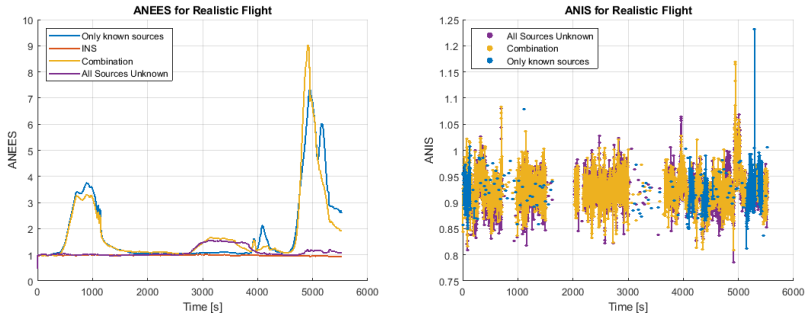

(a) *ANEES for the 4D vehicle state.* ***(b)*** *ANIS for the filter.*

Figure 4.26: *Test of filter consistency using ANEES and ANIS.*

The plot of the ANEES shows that the INS stays at a value around 1 for the whole simulation, which indicates that the variable Q_k has been properly tuned. The ANEES for when only unknown sources are used is also low throughout the simulation, with a peak of 1.5 halfway into the flight. However, for the cases where known sources are utilised, the ANEES is much more fluctuating and has high

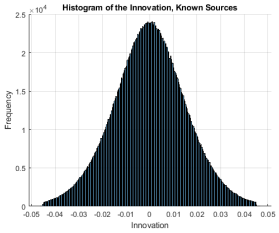

(a) Innovation for known sources.

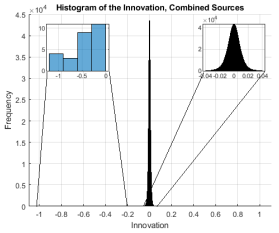

(b) Innovation for combined sources.

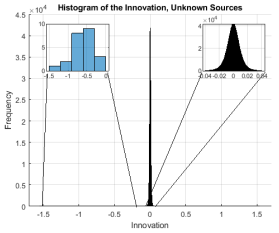

(c) Innovation for unknown sources.

Figure 4.27: *Histograms of the innovations for the different cases.*

spikes, indicating that the estimated covariance has not matched the actual state estimation error. When compared to the plot of the RMSE, one can see that the estimation error has spikes that seems to correlate to the spikes in the ANEES. The error propagates faster than the INS drift in these cases, indicating a too low estimated covariance. The problem only appears when known sources are used and in specific cases. When resampling the map, the peaks appear at new locations which indicate that the problem occurs in certain parts of the map. One theory is that the problem is caused by the fact that the filter uncertainty can only be increased by the INS, which means that if the measurement conditions rapidly worsen, the estimated covariance can not be increased to compensate for this. This could happen if the aircraft suddenly passes through a bad part of the map, for instance in between two sources, where the localisation performance is reduced, as shown in Section 4.2.1. This could cause linearisation errors, and the effects are probably more visible when using known sources as these measurements are more trusted than the unknown sources and therefore have a higher impact on the aircraft state. This is not a good behaviour, but the spikes seems to be temporary and the ANEES does recover to low levels after a short while. The cause of the spikes needs to be further investigated in order to achieve a fully robust system.

Figure 4.26b shows that the ANIS values for all different cases are centred around 0.95 and do not fluctuate much. This indicates that the estimation of the innovation covariance is good but slightly high, which likely is a result of the outlier rejection, as discussed in Section 4.3. When the innovations are further analysed, one can see that innovation mean is approximately zero for all tested cases, and show clear indications of being normally distributed with approximately the same variance for all tests. However, when using unknown sources, the amount of outlier values are increased, which might be caused by the outlier rejection letting more noisy measurements through. Though, when comparing to the results presented in Section 4.3, where the same type of histogram has been presented for the case when not using outlier rejection, one can see that the amount of outlier values have significantly decreased. Considering the very low frequencies

in the outlier regions, the innovation can arguably be accepted as white for the finite amount of data.

4.7 Computational Complexity

The computational complexity is analysed by comparing the average computational time of one measurement update for the different algorithms when varying the number of observed sources. The computational time for the two different initiation methods in Section 4.4 are also compared.

When analysing the computational time in Figure 4.28, one can see that the time seems to increase when the amount of sources is increased. This is slightly less noticeable when using known sources which are not included in the state. The computational time when sources are included in the state is notably longer than when not. The time is about twice as long in the beginning and about 8 times as long in the end. Also, using unknown sources takes longer time than using known sources, even if they are included in the state.

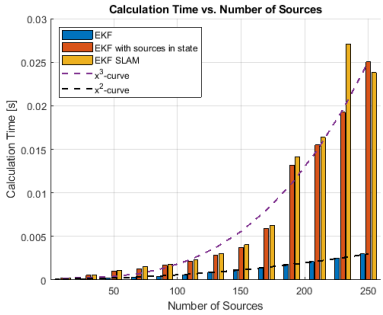

Figure 4.28: *Computational time when varying the number of observed sources. "EKF with sources in state" represent the case when all sources are known but are included in the state as described in Section 3.6. EKF and EKF SLAM is used when the sources are known and unknown respectively. The x^2- and x^3-curves are fitted when there are 250 sources for EKF without respectively with sources in state.*

It is reasonable that it takes longer time when sources are included in the state than when they are not. This is mainly because the state covariance matrix increases with each new source while matrix multiplications scale as n^3. It is also reasonable that the EKF SLAM takes longer time when the sources are unknown compared to known. When the sources are known, they are instantly initialised in the state with a predefined starting covariance. This can be compared to when they are unknown, where the initial position and covariance first need to be estimated using the NLS method before they can be added to the state. Even though this only increases the time during the initialisation, it results in a longer average

time.

The computational time should theoretically increase cubically with the state dimension for the EKF and EKF SLAM algorithms and quadratically with the number measurements, if the sparseness of the H-matrix is utilised [13]. From the results, it is seen that the computational time increases when increasing the number of sources and that the trend looks cubical when the sources are in the state and quadratic when not. This coincides with the theory since the state is unchanged when the sources are not in the state. However, even for sources in the state, the trend looks more linear in the beginning. This could be caused by the fact that the prediction step in SLAM algorithm scales linear with the number of landmarks, due to the separation between vehicle and landmark states [15]. There are also other calculations apart from the regular EKF and EKF SLAM, such as the outlier rejection. These could thereby damp the characteristics of a cubical increase in the beginning if their complexities are lower. This effect would however be negligible when the number of sources approach infinity. The inconsistencies, for example the big jump between 170 and 190 sources, is possibly caused by the fact that Matlab can perform calculations and save data differently depending on the size of the data, and interference from other processes can occur some times during the tests.

The results in Figure 4.29 show a clear increase in the computational time for the case when NLS is used compared to the AM method, especially in the early stage of the simulation. By comparing the time against the number of sources initialised in the filter, a higher time in the beginning seems to coincide with more sources in the initialisation stage. It then drops notably when the last landmark has been added. After this, the computational time stabilises at approximately the same level for both cases.

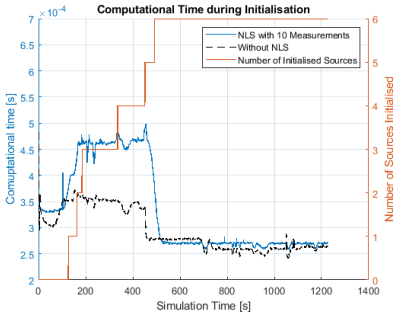

Figure 4.29: *Computational time during the simulation when using an initiation with and without NLS (AM method). The total number of initialised sources is also displayed.*

A longer computational time when using the NLS initialisation is reasonable

since this approach uses the AM method to get a first guess for the Gauss Newton algorithm, which in turn also takes time. A longer computational time in the beginning correlates with the number of initiated sources. This indicates that the initialisation process takes longer time when more sources are being initialised, which is reasonable. Especially since the computational time drops when all sources have been initialised.

5

Concluding Remarks

In this chapter, the results from the simulation study are summarised. Also, some recommended future work needed is discussed.

5.1 Summary

Using SOO for aircraft positioning has proven to be an alternative to using an unassisted INS in GNSS denied environments. Instead of an unlimited drift in position error, the error can be stabilised, even if the signal source positions are unknown. In realistic scenarios, using the standard parameters in this thesis, the best achieved RMSE is around 100 meters. However, the performance is highly affected by a number of factors.

SOO-DOA Localisation for Known Source Locations

The DOA localisation performance is mainly dependent on the measurement noise, the measurement update frequency and the availability of sources, if the signal source locations are known. The estimation error seems to scale linearly with the distance to sources while the error drops with a diminishing effect when the amount of sources used simultaneously is increased. Measurement outliers have also been proven to have a big impact on the performance and thus, good outlier rejection is needed. The method for outlier rejection used in this thesis effectively reduces the impact of measurement outliers in the filter and thus increases the robustness. Furthermore, the absolute position of the aircraft can be reestablished even after a substantial amount of position drift has occurred. Therefore, knowledge about source locations should be incorporated whenever possible. However, the availability of SOO from known source locations is prob-

ably limited and the number of unknown sources is often larger. The EKF indicates consistency, as the ANIS values are close to 1 for the tested cases and the innovation can be accepted as white as it has zero mean and is normally distributed. The ANEES is also close to 1 in most cases, however, the value is fluctuating in some specific scenarios when known sources are used. Thus, further work is needed in order to achieve an even more robust system.

SOO-DOA Localisation for Unknown Source Locations

If unknown sources are to be utilised, several further factors are important in order to achieve a robust system with good performance. The initialisation of new sources is very important since a good initial estimate is needed for them to make a difference in aircraft position estimate. Their initial covariance is especially important since estimates with a too high covariance does not seem to contribute to an improvement of aircraft position estimate, while a too low covariance on sources with bad initial estimates can deform the map and cause an even worse aircraft position estimate. With this background, reasonable covariance estimates is an important quality for the filter and a key factor in order to achieve a robust system. Moreover, the method for outlier rejection cannot be utilised before landmarks have been added to the state in the SLAM case and thus, the initialisation method also needs to be robust against outliers. A NLS method which utilises several measurements before a source is initialised in the filter seems to work in most cases. However, large outliers might still be difficult to handle.

The SLAM algorithm is also greatly influenced by the number of observations from initialised sources and has thereby shown to yield limited improvements in performance compared to the unassisted INS when quickly passing through different environments with new sources. This means that the choice of trajectory is an important factor for the SLAM performance, and the effect is also amplified by the delayed initialisation as it takes longer time before new sources are initialised. When entering new areas after a previous drift in estimation error, the error only seems to stabilise and not decrease, since new landmarks are initialised with an offset caused by the error in aircraft position. Sources with unknown locations could however be very useful when flying in the same area for a longer period of time or revisiting previously discovered areas. The EKF SLAM also indicates filter consistency and do not seem to have the same problem with a fluctuating ANEES when only unknown source locations are used.

Using a combination of known and unknown source locations can improve the performance, as the benefit of using many sources can be combined with the fact that an absolute position can be established when known source locations are utilised. This is especially important before the unknown sources have converged to a decent estimate, as a more stable localisation solution is obtained compared to using only unknown source locations.

Computational Time

The computational time scales cubically with the number of states used in the filter, and approximately quadratically with the number of measurements used in the EKF. The time is longer when using unknown source locations because of the initialisation process and is increased when the NLS method is used for initialisation compared to when only artificial measurements are used.

5.2 Future Work

The initiation of new sources has been proven to affect the performance of the SLAM algorithm significantly and is therefore an aspect that could be studied further. A good start would be some sort of outlier rejection that can detect outliers on measurements not yet initialised in the filter, something not possible with the current rejection method. Instead, this is handled by using several measurements and by adding extra uncertainty to the landmarks. If the initial certainty could be increased, the sources would increase the performance of the aircraft position faster. This is also true if an undelayed initiation method is used. An example is to investigate the possibility of using measurements for the elevation angles to roughly estimate the distance between sources and the aircraft. By doing this, only one measurement is required to initialise a landmark if the altitude is known. Furthermore, a separate filter for landmarks could be implemented to increase source estimation accuracy before they are integrated in the filter for the aircraft position. However, this would also delay the initialisation process. The benefits of such an approach is that bad initial estimates can be improved without affecting the aircraft state. Currently this does not happen since the outlier rejection classifies their measurements as outliers, meaning that their position estimate remain unchanged since no measurements comes through.

Regarding the filter consistency, the ANEES showed that the estimated covariance does not match the actual variance of the estimation error in all cases. Thus, further investigation is needed in order to be able to fully trust the covariance provided by the filter.

To save memory in the aircraft, a limitation of the number of states saved in the filter could be implemented. In a real application, it is unnecessary to save sources not used for a long time or which have low certainties. In [26], reducing the map is proven to significantly increase the computational efficiency while the statistical consistency and error in estimated vehicle position are not significantly compromised.

The minimum distance to sources can also be further investigated since the value of 1 km as used in this thesis was chosen without a concrete analysis. One pos-

sibility could be to have a minimum value depending on the uncertainty of each individual source. This is an important parameter since without a minimum, it was discovered that sources could be initiated on the wrong side of the aircraft which caused significant problems. Using a maximum distance could also be investigated to see if the performance is affected, as the localisation error seem to linearly increase with the distance to the sources.

Bibliography

[1] Paul Groves. *Principles of GNSS, Inertial, and Multisensor Integrated Navigation Systems, Second Edition*. 2013.

[2] Aron Pinker and Charles Smith. Vulnerability of the GPS signal to jamming. *GPS Solutions*, 3: 19–27, 1999. doi: 10.1007/PL00012788.

[3] Joshua J. Morales and Zaher M. Kassas. Tightly coupled inertial navigation system with signals of opportunity aiding. *IEEE Transactions on Aerospace and Electronic Systems*, 57(3):1930–1948, 2021. doi: 10.1109/TAES.2021.3054067.

[4] John F. Raquet, Mikel M. Miller, and Thao Q. Nguyen. Issues and approaches for navigation using signals of opportunity. In *Proceedings of the 2007 National Technical Meeting of The Institute of Navigation*, pages 1073–1080, 2007. doi: 10.14339/RTO-MP-SET-104-09-pdf.

[5] Adrian Winter, Nadezda Sokolova, Aiden J. Morrison, and Tor A. Johansen. GNSS-denied navigation using direction of arrival from low-cost software defined radios and signals of opportunity. *European Conference for Aeronautics and Space Sciences*, pages 1–1, 2022. doi: 10.13009/eucass2022-7461.

[6] Alfonso Farina. Target tracking with bearings – only measurements. *Signal Processing*, 78(1): 61–78, 1999. ISSN 0165-1684. doi: 10.1016/S0165-1684(99)00047-X.

[7] Gustaf Hendeby, Rickard Karlsson, Fredrik Gustafsson, and Neil Gordon. Recursive triangulation using bearings-only sensors. In *Proceedings of the 2006 IEE Seminar on Target Tracking: Algorithms and Applications*, pages 3–10. Institution of Electrical Engineers (IEE), 2006.

[8] Yankui Zhang, Daming Wang, Weijia Cui, Jiangdong You, Hao Li, and Fei Liu. DOA-based localization method with multiple screening k-means clustering for multiple sources. *Wireless Communications and Mobile Computing*, vol. 2019, 2019. doi: 10.1155/2019/5643752.

[9] Bisma Amjad, Qasim Z. Ahmed, Pavlos I. Lazaridis, Maryam Hafeez, Faheem A. Khan, and Zaharias D. Zaharis. Radio SLAM: A review on radio-based simultaneous localization and mapping. *IEEE Access*, pages 1–1, 2023. doi: 10.1109/ACCESS.2023.3237330.

[10] Alfred Dahlin. Simultaneous localization and mapping for an unmanned aerial vehicle using radar and radio transmitters. Technical Report Master Thesis LiTH-ISY-EX–14/4794–SE, Department of Electrical Engineering Linköping University, 581 83, Linköping, Sweden, 2014.

[11] BAE Systems. Navigation via signals of opportunity (NAVSOP). `https://www.baesystems.com/en/product/navigation-via-signals-of-opportunity-navsop`. Accessed: 2023-02-02.

[12] U.S. Department of Transportation Federal Avaiation Administration. *Instrument Flying Handbook*. Skyhorse Publishing, Inc., 2017.

[13] Fredrik Gustafsson. *Statistical Sensor Fusion*. Studentlitteratur, 3rd edition, 2018.

[14] H. Durrant-Whyte and T. Bailey. Simultaneous localization and mapping: Part I. *IEEE Robotics and Automation Magazine*, 13(2):99–110, 2006. doi: 10.1109/MRA.2006.1638022.

[15] T. Bailey and H. Durrant-Whyte. Simultaneous localization and mapping (SLAM): Part II. *IEEE Robotics and Automation Magazine*, 13(3):108–117, 2006. doi: 10.1109/MRA.2006.1678144.

[16] J. Sola, A. Monin, M. Devy, and T. Lemaire. Undelayed initialization in bearing only SLAM. In *2005 IEEE/RSJ International Conference on Intelligent Robots and Systems*, pages 2499–2504, 2005. doi: 10.1109/IROS.2005.1545392.

[17] James Moody. What does RMSE really mean. `https://towardsdatascience.com/what-does-rmse-really-mean-806b65f2e48e`, 2019. Accessed: 2023-02-21.

[18] Yaakov Bar-Shalom, Li Rong, and Thiagalingam Kirubarajan. *Estimation with Applications to Tracking and Navigation*. John Wiley & Sons, Inc, 2001.

[19] Simmons Adam. Cell tower range: How far do they reach? `https://dgtlinfra.com/cell-tower-range-how-far-reach/`, 10 2022. Accessed: 2023-05-02.

[20] A. Devasthale and L. Norin. The large-scale spatio-temporal variability of precipitation over sweden observed from the weather radar network. 06 2014. doi: 10.5194/amt-7-1605-2014.

[21] Christian Wolff. Air surveillance radar. `https://www.radartutorial.eu/02.basics/rp31.en.html`, n. d. Accessed: 2023-05-16.

[22] Saab AB. Giraffe 4a. `https://www.saab.com/products/giraffe-4a`, n. d. Accessed: 2023-04-25.

[23] Telia. Täckningskartor. `https://www.telia.se/privat/support/tackningskartor`, n. d. Accessed: 2023-05-02.

[24] A. Huuskonen, E. Saltikoff, and I. Holleman. The Operational Weather Radar Network in Europe. *American Meterology Society*, 95(6):897–907, 06 2014. doi: 10.1175/BAMS-D-12-00216.1.

[25] Samuel Blackman and Robert Popoli. *Design and Analysis of Modern Tracking Systems*. Artech House Radar Library, 1999.

[26] G. Dissanayake, H. Durrant-Whyte, and T. Bailey. A computationally efficient solution to the simultaneous localisation and map building (SLAM) problem. In *Proceedings 2000 ICRA. Millennium Conference. IEEE International Conference on Robotics and Automation. Symposia Proceedings (Cat. No.00CH37065)*, volume 2, pages 1009–1014 vol.2, 2000. doi: 10.1109/ROBOT.2000.844732.